

AD-A158 999

THE EQUILIBRIUM MIXED LAYER DEPTH IN THE TROPICAL ATLANTIC THE ROTATION S. (U) NAVAL POSTGRADUATE SCHOOL MONTEREY CA J F GASPAR JUN 85

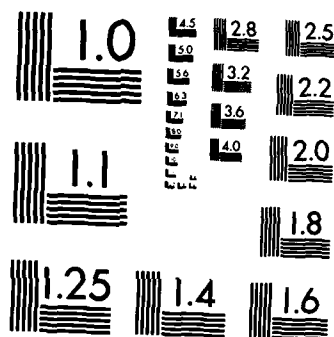
1/1

UNCLASSIFIED

F/G 8/10

NL

[illegible]



MICROCOPY RESOLUTION TEST CHART
NATIONAL BUREAU OF STANDARDS-1963-A

2

NAVAL POSTGRADUATE SCHOOL

Monterey, California



DTIC
ELECTE
SEP 12 1985
S A D

THESIS

THE EQUILIBRIUM MIXED LAYER DEPTH IN THE TROPICAL
ATLANTIC: THE ROTATION STRESS AND PENETRATION
OF RADIATION EFFECTS

by

Joaquim Filipe Figueiredo Alves Gaspar

June 1985

Thesis Advisor:

Roland Garwood

Approved for public release; distribution is unlimited.

AD-A158 999

DTIC FILE COPY

85 9 10 000

REPORT DOCUMENTATION PAGE		READ INSTRUCTIONS BEFORE COMPLETING FORM
1. REPORT NUMBER	2. GOVT ACCESSION NO.	3. RECIPIENT'S CATALOG NUMBER
4. TITLE (and Subtitle) The Equilibrium Mixed Layer Depth in the Tropical Atlantic : the Rotation Stress and Penetration of Radiation Effects		5. TYPE OF REPORT & PERIOD COVERED Master's Thesis June, 1985
		6. PERFORMING ORG. REPORT NUMBER
7. AUTHOR(s) Joaquim Filipe Figueiredo Alves Gaspar		8. CONTRACT OR GRANT NUMBER(s)
9. PERFORMING ORGANIZATION NAME AND ADDRESS Naval Postgraduate School Monterey, California 93943-5100		10. PROGRAM ELEMENT, PROJECT, TASK AREA & WORK UNIT NUMBERS
11. CONTROLLING OFFICE NAME AND ADDRESS Naval Postgraduate School Monterey, California 93943-5100		12. REPORT DATE June, 1985
		13. NUMBER OF PAGES 76
14. MONITORING AGENCY NAME & ADDRESS (if different from Controlling Office)		15. SECURITY CLASS. (of this report)
		15a. DECLASSIFICATION/DOWNGRADING SCHEDULE
16. DISTRIBUTION STATEMENT (of this Report) Approved for public release; distribution is unlimited		
17. DISTRIBUTION STATEMENT (of the abstract entered in Block 20, if different from Report)		
18. SUPPLEMENTARY NOTES		
19. KEY WORDS (Continue on reverse side if necessary and identify by block number) Planetary boundary layer, oceanic mixed layer		
20. ABSTRACT (Continue on reverse side if necessary and identify by block number) The effects of the rotation stress mechanism and the penetration of short-wave radiation below the sea-surface are examined in determining a one-dimensional equilibrium mixed layer depth. Starting with the Obukhov-scale equilibrium theory for the surface ocean boundary layer, a revised equilibrium theory, which includes rotation stress and radiation effects, is presented. This new theory is applied using climatological boundary conditions for the tropical Atlantic, and the results		

20.(cont)

are compared with the observed climatological mixed layer depth.

In general, the response of the revised model is an improvement over the Obukhov theory alone. Because the quality of the results are limited by uncertainties in the boundary conditions, no detailed evaluation of the model response is justifiable. However, it is concluded here that the physical mechanisms of rotation stress and penetration of radiation are important in determining a steady-state equilibrium depth of mixing for the tropical Atlantic.

Accession	
NTIS Grant	
DTIC TAB	
Unannounced	
Justification	
By	
Distribution/	
Availability Codes	
Dist	
A-1	



Approved for public release ; distribution is unlimited

The Equilibrium Mixed Layer Depth in the Tropical Atlantic :
the Rotation Stress and Penetration of Radiation Effects

by

Joaquim Filipe Figueiredo Alves Gaspar
Lieutenant Commander, Portuguese Navy

Submitted in partial fulfillment of the
requirements for the degree of

MASTER OF SCIENCE IN OCEANOGRAPHY

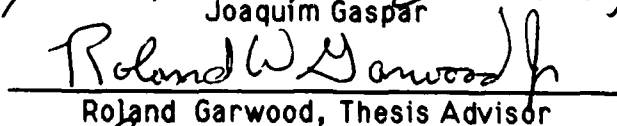
from the

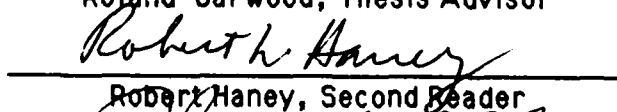
NAVAL POSTGRADUATE SCHOOL
June, 1985

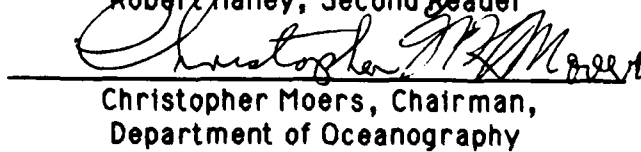
Author :

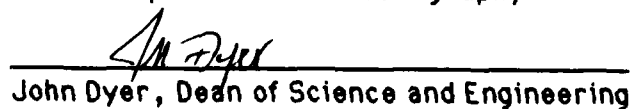

Joaquim Gaspar

Approved by :


Roland Garwood, Thesis Advisor


Robert Haney, Second Reader


Christopher Moers, Chairman,
Department of Oceanography


John Dyer, Dean of Science and Engineering

ABSTRACT

1. The effects of the rotation stress mechanism and the penetration of short-wave radiation below the sea surface are examined in determining a one-dimensional equilibrium mixed layer depth. Starting with the Obukhov-scale equilibrium theory for the surface ocean boundary layer, a revised equilibrium theory, which includes rotation stress and radiation effects, is presented. This new theory is applied using climatological boundary conditions for the tropical Atlantic, and the results are compared with the observed climatological mixed layer depth.

In general, the response of the revised model is an improvement over the Obukhov theory alone. Because the quality of the results ⁽⁵⁾are limited by uncertainties in the boundary conditions, no detailed evaluation of the model response is justifiable. However, it is concluded here that the physical mechanisms of rotation stress and penetration of radiation are important in determining a steady-state equilibrium depth of mixing for the tropical Atlantic.

Key words: Planetary boundary layer; Air-water interactions; Radiation; Rotation stress; Mixed layer depth.

TABLE OF CONTENTS

I. INTRODUCTION	8
II. THE DYNAMICS OF MIXING	10
A. THE TURBULENT KINETIC ENERGY BUDGET	10
1. Shear Production of Turbulence	10
2. The Buoyancy Flux.....	12
3. Turbulence Diffusion.....	14
4. Dissipation.....	14
B. EQUILIBRIUM DEPTH OF MIXING	15
1. The Obukhov Length Scale.....	17
2. The Kraus and Turner Steady-State Model	18
III. THE REVISED STEADY-STATE MODEL	20
A. EFFECT OF THE PENETRATING RADIATION ON THE BUOYANCY FLUX ...	21
B. THE ROTATION STRESS MECHANISM	23
C. EQUILIBRIUM DEPTH OF MIXING	25
IV. THE EQUILIBRIUM MIXED LAYER IN THE TROPICAL ATLANTIC	29
A. THE BOUNDARY CONDITIONS	29
1. The Observed Mixed Layer Depth.....	29
2. The Surface Heat Flux.....	31
3. The Surface Wind Stress.....	32
4. Steady-State <i>versus</i> Time-Dependent Solutions.....	32
B. METHOD OF MODEL TUNING.....	38
C. RESULTS	42

1. Equator.....	42
2. 10 degrees North.....	50
V. CONCLUSIONS	58
LIST OF REFERENCES	61
APPENDIX A - MODEL OUTPUT	63
APPENDIX B - COMPUTER PROGRAMS	65
INITIAL DISTRIBUTION LIST	75

ACKNOWLEDGMENT

I dedicate this work to all those who, during my learning experience in the Naval Postgraduate School, kept me aware of the fact that the best way to fully understand the mechanics of the wheel is to reinvent it.

1. INTRODUCTION

The study of the oceanic turbulent boundary layer is a relatively recent field in Physical Oceanography. Since the pioneering work of Kraus and Turner (1967), a significant effort has been made in understanding and modelling the dynamics of turbulent mixing in the oceans. However, the basic contributions made by those authors still provide the theoretical foundation for much of the current research.

The oceanic boundary layer or mixed layer is considered in this study to be the fully turbulent region that is bounded above by the air-ocean interface, and it is where the temperature and salinity are usually observed to be fairly well mixed. Below, the mixed layer is assumed to be bounded by a dynamically stable thermocline.

The study of the top few tens of meters of the ocean is of considerable scientific interest. Ekman pumping effects, originating in the mixed layer by the action of wind forcing, considerably influences the dynamics of the lower levels and the interior circulation in general. Also, the interaction between the oceanic and atmospheric boundary layers is an essential mechanism which must be considered when making medium and long-range weather forecasts, since a large part of the atmospheric energy supply comes from the heat exchanged between these layers. Additionally, this is the region of primary biological productivity, which is of significant economic importance. An important military application is, on the other hand, the modelling of acoustic propagation in the oceans.

Most of the physics behind existing models of the oceanic mixed layer are based on the flux form of the Navier-Stokes equations of motion, with the Boussinesq approximation. One-dimensional versions, like the one which is treated in this study, further assume the horizontal gradients of the mean fields to be negligible. For a steady-state situation, this will lead to the basic energy balance, as stated by Kraus and Turner (1967), between the work done by the wind stress and the surface heating, in defining an equilibrium depth of mixing. However, a usually neglected term in the turbulent kinetic energy budgets, the planetary rotation term, was recently examined by Garwood *et al.* (1985a). They suggest a new formulation for the equilibrium mixed layer depth, which basically describes the interaction between the zonal Reynolds stresses and the northward component of the planetary rotation. This new formulation might partially explain the zonal variation of the observed mixed layer depth in the Tropical Pacific and Atlantic Oceans.

The goal of this study is to apply the Kraus and Turner (1967) and the Garwood *et al.* (1985b) one-dimensional, steady-state models on a relatively broad grid with realistic boundary conditions in the Equatorial and Tropical Atlantic Ocean, and to compare the resulting diagnostic mixed layer depths with the observed mixed layer depths. In this way, insight may be gained into the relative importance of the physical mechanisms involved. Also, we should be able to identify the regions and time of the year where the turbulent boundary layer can be represented realistically by such simple steady-state equilibrium models.

II. THE DYNAMICS OF MIXING

A. THE TURBULENT KINETIC ENERGY BUDGET

In the presence of a constant wind stress and a downward surface heat flux, the steady-state, one-dimensional turbulent kinetic energy (TKE) budget is, assuming no vertical advection :

$$0 = \partial/\partial t [\bar{E}/2] = -\overline{u'w'} \partial\bar{u}/\partial z - \overline{v'w'} \partial\bar{v}/\partial z + \overline{b'w'} - \partial/\partial z [\overline{w'(E/2)} + \overline{w'p'}/\rho] - d, \quad (2.1)$$

where $E/2$ is the TKE, $-\overline{u'w'} \partial\bar{u}/\partial z - \overline{v'w'} \partial\bar{v}/\partial z$ represents the production of kinetic energy associated with the vertical shear in the horizontal flow induced by the wind stress, $\overline{b'w'}$ is the buoyancy flux, $-\partial/\partial z [\overline{w'(E/2)} + \overline{w'p'}/\rho]$ is the turbulent diffusion and d is the dissipation. With no loss of generality, we shall assume the x -axis to be oriented downstream, so that $\bar{v}=0$.

1. Shear Production of Turbulence

Let $\bar{u}(z)$ be some monotonic function of z between the surface, $z=0$, and the bottom of the mixed layer, $z=-h$. For the sake of simplicity, it is further assumed that $\bar{u}(-h)=0$, since no entrainment is allowed.

Consider now (Fig. 1a) that some particle initially at 1 is displaced to some position 2 by means of a positive turbulent vertical velocity w' . Because $\partial\bar{u}/\partial z \geq 0$, the particle will acquire a negative turbulent horizontal velocity u' and, then, $u'w'$ will be less than zero at 2. Alternatively, a

particle initially at 1, which is displaced to 3 by means of a negative vertical turbulent velocity w' , will acquire a positive horizontal turbulent velocity u' and, again, $u'w'$ will be negative. In both situations, the shear production term $-u'w' \partial \bar{u} / \partial z$ will be positive, and when this physical process is averaged over the whole turbulent layer, it will tend to increase the TKE at the expense of the mean kinetic energy. Formally,

$$-\overline{u'w'} \partial \bar{u} / \partial z > 0.$$

Evaluated over the mixed layer, the shear production will be:

$$G \equiv \int_{-h}^0 -\overline{u'w'} \partial \bar{u} / \partial z \, dz = \langle -\overline{u'w'} \rangle [\bar{u}(0) - \bar{u}(-h)], \quad (2.2)$$

where $\langle \rangle$ represents a vertical average. At the bottom of the mixed layer, and under the assumption of no entrainment, $-\overline{u'w'}(-h)$ is zero. Then, disregarding nondimensional constants, $\langle -\overline{u'w'} \rangle$ is of order $-\overline{u'w'}(0)$. Also, we have already assumed $\bar{u}(-h)$ to be zero. Thus,

$$G = -\overline{u'w'}(0) \bar{u}(0). \quad (2.3)$$

Furthermore, the Reynold stress $-\overline{u'w'}(0)$ can be written

$$|-\overline{u'w'}(0)| = |\tau|/\rho, \quad (2.4)$$

where ρ is a typical sea water density and τ is the surface wind stress. Finally, (2.3) is rewritten as

$$G = \bar{u}(0)|\tau|/\rho. \quad (2.5)$$

2. The Buoyancy Flux

Under the influence of surface heating, there will be a tendency for stratification, and mixing will only occur in the presence of wind stirring. In this case, the less dense particles near the surface will mix with the

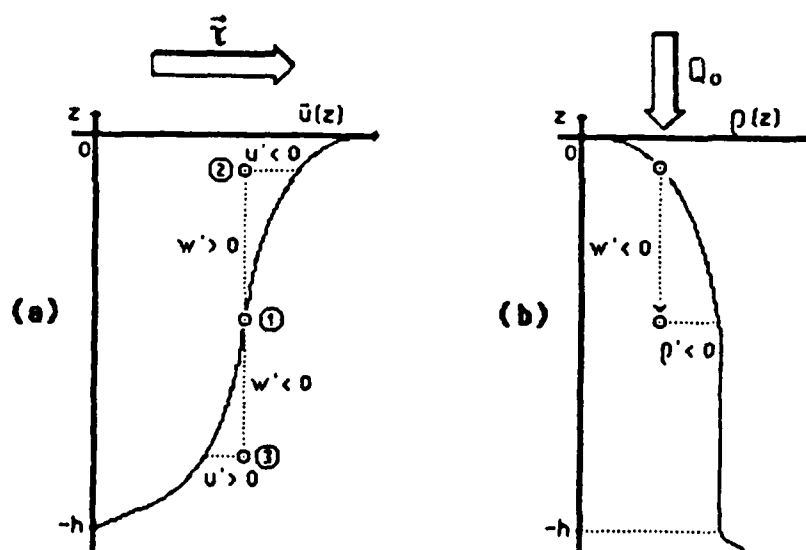


Fig. 1. (a) Shear production of turbulent kinetic energy, in the presence of wind stress. (b) Buoyant damping of turbulent kinetic energy, in the presence of surface heating.

underlying water only at the expense of the wind-generated turbulence, thus converting TKE into potential energy (Fig. 1b). This means that, on the average, the buoyancy flux $-\overline{b'w'}$ will be a sink term in the TKE budget. The equilibrium between the effects of wind mixing and surface heating is indeed the fundamental energy balance for any steady-state, one-dimensional mixed layer model, as long as advection is neglected.

To relate the buoyancy flux to the surface heat flux Q_0 we apply the linearized equation of state and obtain:

$$\overline{b'w'} = \alpha g \overline{T'w'}, \quad (2.6)$$

where α is the thermal expansion coefficient, g is the acceleration of gravity and $\overline{T'w'}$ is the temperature flux. It can further be shown that, assuming vertical homogeneity in the mean temperature T , $\overline{T'w'}$ will be linear over the mixed layer, and

$$\overline{T'w'}(0) = -Q_0/(\rho C_p), \quad (2.7)$$

where Q_0 , the surface heat flux is positive downward.

Integrating the buoyancy flux over the mixed layer,

$$B \equiv \int_{-h}^0 \overline{b'w'} dz = \alpha g \int_{-h}^0 \overline{T'w'} dz = \alpha g h [\overline{T'w'}(0) + \overline{T'w'}(-h)]/2, \quad (2.8)$$

where h is the mixed layer depth. Because no entrainment is assumed, $\overline{T'w'}(-h)=0$. Thus,

$$B = -\alpha g h Q_0 / (2\rho C_p). \quad (2.9)$$

This simple model for the vertically integrated buoyancy flux also requires the assumption that the net solar radiation be completely absorbed at the surface. We will see in the following sections that this assumption is incorrect when the vertical scale of penetration of radiation below the surface is comparable to the vertical scale of turbulent mixing. The effect of the penetration of radiation is expected to be relevant in optically clear oceanic waters and in summertime conditions, when the mixed layer is relatively shallow. In those situations, the net downward buoyancy flux may be significantly reduced, causing the resultant depth of mixing to be significantly increased.

3. Turbulent Diffusion

Although the diffusion of turbulence is an essential mechanism in transporting TKE downwards from the upper levels, it does not constitute, by itself, a source or sink of turbulence, which means that its net value over the mixed layer must vanish. Formally,

$$\int_{-h}^0 -\partial/\partial z [\overline{w'(E/2) + w'p'/\rho}] dz = 0. \quad (2.10)$$

4. Dissipation

Early mixed layer models, including the Kraus and Turner (1967) model, recognized the existence of dissipation. However, they considered its influence to be negligible, given the relatively large length scale of turbulent

mixing. Indeed, a less careful scale analysis of the TKE budget seems to support the approximation. More recent models, however, include dissipation in the mechanical energy budget, either as a fraction of the wind-stress production or as a fraction of the net TKE production. Although viscous dissipation may be neglected when dealing with turbulent eddies of length scales of order of the mixed layer depth, the dynamic interaction between those eddies produces other eddies of smaller and smaller dimensions, where the role of dissipation may finally dominate. This fact is easily understood with the analysis of a spectrum of turbulence, where it can be verified that the mechanical energy drops rapidly above a limiting frequency (Tennekes and Lumley, 1962).

If such a dissipation mechanism is included in the TKE budget by parameterization, for example as a fraction of the TKE production, we will see in the following sections that the Kraus and Turner model is still usable, since no additional degree of freedom is required. That was the approach of Geisler and Kraus (1969), Niller (1975) and others.

For now, we will just define the vertically integrated dissipation D as:

$$D \equiv \int_{-h}^0 d \, dz. \quad (2.11)$$

B. EQUILIBRIUM DEPTH OF MIXING

From the results of the previous section, the vertically integrated TKE budget can be written as

$$B + G - D = 0, \quad (2.12)$$

where

$$B = - \alpha g h Q_0 / (\rho C_p)$$

and

$$G = \bar{u}(0) |\tau| / \rho .$$

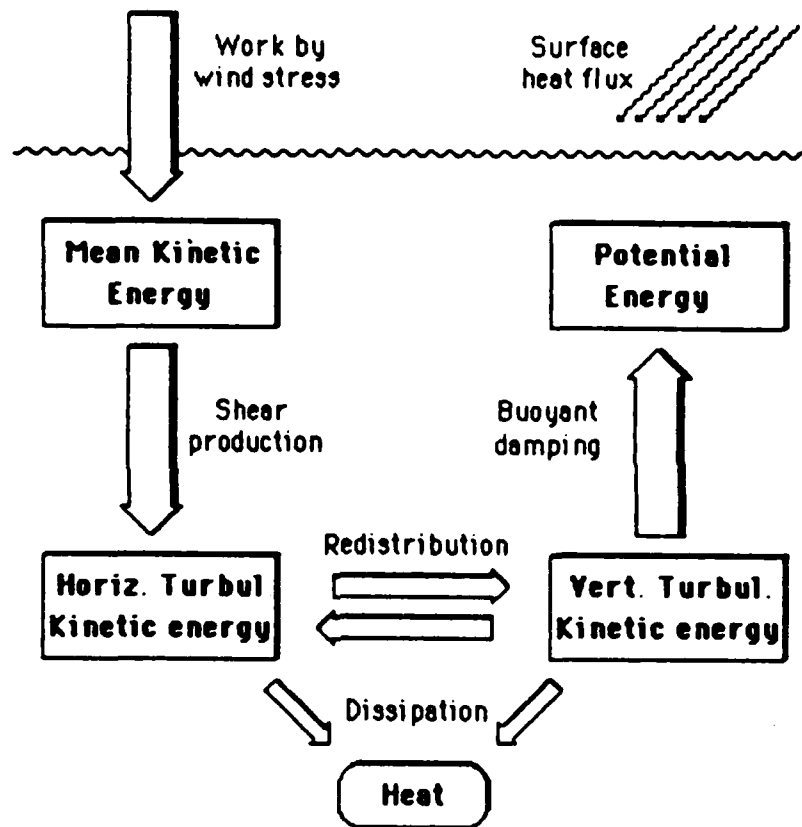


Fig. 2. The one-dimensional mixed layer equilibrium. The "redistribution" effects include the pressure redistribution and the rotation stress mechanism.

Equation (2.12) illustrates the basic steady-state balance between the work done by the wind stress and the buoyant damping (Fig. 2). Note that, because of turbulent mixing, the mean flow will tend to be vertically homogeneous, except near the surface, where turbulence is generated, and near the bottom of the mixed layer, where it falls to zero. Also, the mean temperature profile will tend to be homogeneous. Thus, the mixed layer potential energy will approach its theoretical maximum value.

In Fig. 2 an additional mechanism is illustrated. This process, called "redistribution", does not appear in the TKE budget, since its constituent terms sum to zero when the three spatial components of the kinetic energy budget are added. Redistribution consists of two parts: the pressure redistribution and the planetary rotation. Their roles are to exchange TKE among the x - y - z directions, tending to restore the system's isotropy. In section III, the planetary rotation term will be shown to have a fundamental role in determining the equilibrium mixed layer depth for the Garwood *et al.* (1985a) steady-state model.

1. The Obukhov Length Scale

We have seen that, if dissipation is parameterized in terms of the other basic turbulent variables, the steadiness of the mixed layer depth will depend on the surface boundary conditions, i.e., the surface wind stress and the surface heat flux. This is equivalent to setting $G/B = \text{constant}$.

We will now define a velocity scale u_* , which is representative of the typical turbulent speed of the largest eddies in a wind-driven mixed layer:

$$u_*^2 = |\tau|/\rho . \quad (2.13)$$

Because $\bar{u}(0)$ depends linearly on the wind speed and, thus, on the surface wind stress, the shear production term G in equation (2.5) can be scaled as

$$G \sim u_*^3. \quad (2.14)$$

Combining (2.9) and (2.12-14), and setting $-G/B = 1$, the Obukhov length scale is defined as

$$L \equiv h = 2 \rho C_p u_*^3 / (\alpha g Q_0). \quad (2.15)$$

Physically, L represents the scale of maximum depth of turbulent mixing, given the surface boundary conditions of wind stress and heat flux, for an equilibrium mixed layer with no advection present.

2. The Kraus and Turner Steady-State Model

Based on equation (2.12), Kraus and Turner (1967) considered the dissipation to be negligible, so that

$$B + G = 0. \quad (2.16)$$

Also, the vertically integrated shear production G can be written

$$G = u_*^3 = (|\tau|/\rho)^{3/2} \quad (2.17)$$

or

$$G = (\rho_a C_D U^2 / \rho)^{3/2}, \quad (2.18)$$

where C_D is the drag coefficient, ρ_a is the air density and U is the wind speed measured at 10 meters above the surface. Substituting (2.9) and (2.18) into (2.16), the equilibrium depth of mixing is written

$$h = C_1 (\rho C_p / \alpha g Q_0) (\rho_a C_D U^2 / \rho)^{3/2} , \quad (2.19)$$

where C_1 is a dimensionless constant of order 1.

More recent versions of the Kraus and Turner model assume the dissipation D to be proportional to the total TKE production $B+G$, so that equation (2.12) is written as

$$(K + 1)(B + G) = 0, \quad (2.20)$$

where K is a dimensionless constant. As stated earlier, this will lead to the same basic result of equation (2.19), since no additional degree of freedom is included.

III. THE REVISED STEADY STATE MODEL

As noted in section I, the dynamics of the oceanic mixed layer in the equatorial and tropical regions are not fully understood. One of the most apparent but least understood features is the zonal variation of the mixed layer depth.

Some of the discrepancies between the observed mixed layer depths and the predictions made by existing steady-state and one-dimensional models might be explained by the exceptionally strong vertical and horizontal advection which are characteristic of the tropical oceans. Also, the effect of penetration of short wave radiation below the surface is believed to have some importance for relatively shallow mixed layers, especially in the presence of large net solar irradiance. Another physical mechanism, examined by Garwood *et al.* (1985a), involves the interaction between the zonal surface wind stress and the planetary rotation, and it may partially explain the zonal dependence of the steady-state mixed layer depth.

It is beyond the scope of this work to formally treat the effects of advection on the dynamics of the mixed layer, and we shall restrict our study to steady-state situations. However, the other two mechanisms referred to (penetration of radiation and planetary rotation) will be included in the model derived in the following sections.

A. EFFECT OF THE PENETRATING RADIATION ON THE BUOYANCY FLUX

The simplest model for the penetration of radiation below the sea-surface assumes that the net long-wave solar irradiance (infra-red and red) is absorbed at the surface, and the short-wave irradiance decays exponentially with depth. Recent models (Paulson and Simpson, 1977 ; Simpson and Dickey, 1980) also allow for the penetration of long-wave radiation. In both approaches, the predicted vertical profile of absorbed irradiance is sensitive to the values of two empirical parameters: the vertical scale of penetration, which mainly depends on the turbidity of the water, and the short-wave (blue-green) fraction of the net solar irradiance incident on the surface. Because there is only a limited amount of data on the optical properties of the oceans, the values of these empirical parameters will either have to be assumed or adjusted as tuning constants. For that reason, and also because a steady-state model will be applied to large oceanic regions having variable optical properties, the simplest model will be used, i.,e., only the short-wave radiation will be assumed to penetrate below the surface. The vertical profile of the penetrating irradiance will have therefore the following exponential form

$$Q_2(z) = R Q_s e^{-z/\lambda} . \quad (3.1)$$

Here, the downward short-wave irradiance, $Q_2(z)$, is the radiant flux density on a horizontal surface due to contributions from the entire upward hemisphere; Q_s is the net solar irradiance at the surface, R is the short-wave fraction of the net solar irradiance (blue-green), z is the vertical

coordinate, positive upward; and λ is the penetration scale, assumed constant with depth.

Alternatively, the long-wave solar irradiance, assumed to be totally absorbed at the surface, is given by

$$Q_1 = Q_0 - R Q_s, \quad (3.2)$$

where $Q_0 = Q_s - Q_b - Q_h - Q_e$ is the net solar irradiance at the surface, minus the long-wave back radiation, minus the sensible heat flux, minus the latent heat flux.

Assuming horizontal homogeneity of the variables, it can be shown that the effective heat flux Q contributing to the temperature flux over the mixed layer will have the form (Garwood, 1977)

$$Q = Q_1 - \int_{-h}^0 \left[\partial Q_2 / \partial z - 2/h \int_0^s \partial Q_2 / \partial s \, ds \right] dz \quad (3.3)$$

or
$$Q = Q_0 - R Q_s \left[2\lambda/h - e^{-h/\lambda} (1 + 2\lambda/h) \right]. \quad (3.4)$$

For deep mixed layers ($h/\lambda \gg 1$) or, putting $R = 0$, expression (3.4) reduces to $Q = Q_0$, which corresponds to the net heat flux being absorbed at the surface. For shallow mixed layers ($h/\lambda \ll 1$), expression (3.4) reduces to $Q = Q_0 - R Q_s$. Under these circumstances the effect of the penetrating radiation on the effective heat flux is maximum.

It is also apparent from expression (3.4) that, in summertime conditions (small h , large Q_s) and in clear oceanic waters (large λ), Q can be

significantly smaller than Q_0 , thus reducing the buoyancy flux and increasing the vertical extent of the wind generated turbulence.

From expression (2.9), the effective vertically integrated buoyancy flux will then be

$$B = - \alpha g h Q / (2 \rho C_p), \quad (3.5)$$

where Q is given by (3.4).

A. THE ROTATION STRESS MECHANISM

The steady-state turbulent kinetic energy budgets for the three spatial components (x eastward, y northward, z upward), vertically integrated over the mixed layer are:

$$0 = G_x + P_x + \Omega_z h u'v'(0) + \Omega_y h \tau_x / \rho - D/3 \quad (3.6a)$$

$$0 = G_y + P_y - \Omega_z h u'v'(0) - D/3 \quad (3.6b)$$

$$0 = B + P_z - \Omega_y h \tau_x / \rho - D/3. \quad (3.6c)$$

Here G_x and G_y are the horizontal components of the shear production, B is the vertically integrated buoyancy flux, the P_i 's are the components of the vertically integrated turbulent transport, and τ_x is the zonal component of the surface wind-stress. The Ω_i 's are the two spatial components of the planetary rotation and D is the dissipation, assumed to be equally partitioned among components (local isotropy assumed). Since the transport and

planetary rotation terms vanish, the sum of the three above equations simply leads to :

$$B + G - D = 0. \quad (2.12)$$

An additional process, not apparent in (2.12), is evident in equations (3.6). This is the exchange between horizontal and vertical turbulent kinetic energy, in the presence of the zonal wind stress τ_x and the meridional component Ω_y of the planetary rotation. Note that the sign of τ_x will determine whether the term $\Omega_y \tau_x / \rho$ is a source or sink of horizontal turbulent kinetic energy. With easterly winds ($\tau_x < 0$), the horizontal kinetic energy is expected to be enhanced at the expense of the vertical kinetic energy, with a consequent shallowing of the mixed layer. With westerly winds ($\tau_x > 0$), the exchange between the vertical and horizontal components will have the opposite sign, leading to an increase of the vertical extent of turbulent mixing. This mechanism, usually overlooked in planetary boundary layer models, was first examined by Garwood *et al.* (1985b), in an attempt to explain the unusually deep extent of mixing in the central and western Pacific.

If the dissipation is parameterized in terms of the vertical average of the total turbulent kinetic energy, i.e.,

$$D = m_1 \langle \bar{E} \rangle^{3/2}, \quad (3.7)$$

where m_1 and subsequent m_i 's are dimensionless constants, (2.12) can be written

$$G + B - m_1 \langle \bar{E} \rangle^{3/2} = 0. \quad (3.8)$$

Also, the vertical component P_z of the turbulent transport can be parameterized in terms of the vertical average of the TKE. According to Rotta (1951), a first order approximation to the transport term P_z is

$$P_z = m_2 \langle \bar{E} \rangle^{3/2}. \quad (3.9)$$

Substituting (3.9) into (3.6c) and combining with (3.8), will yield a system of two equations which can be solved for the mixed layer depth h and the vertical average of the turbulent kinetic energy $\langle \bar{E} \rangle$, given the surface boundary conditions and the meridional component of the planetary rotation. The predicted value of h will then reflect the interaction between the zonal wind stress and the Earth rotation.

C. EQUILIBRIUM DEPTH OF MIXING

We define

$$L = 2\rho C_p u_*^3 / (\alpha g Q) \quad (3.10)$$

$$G = m_3 u_*^3 \quad (3.11)$$

and

$$\Phi = \Omega_Y \tau_X C_p / (\alpha g Q), \quad (3.12)$$

where the dimensionless parameter Φ is the quotient between the conversion of vertical turbulent kinetic energy by means of the rotation mechanism and the buoyant damping of vertical turbulent kinetic energy. Then, a diagnostic equation for the mixed layer depth can be derived:

$$h = C_1 L / (1 + C_2 \Phi), \quad (3.13)$$

where the non-dimensional constants C_1 and C_2 are related to the m_i 's:

$$C_1 = m_3(m_2/m_1 - 1/3) / (m_2/m_1 + 2/3) \quad (3.14)$$

and
$$C_2 = 2 / (m_2/m_1 + 2/3). \quad (3.15)$$

Note that the effective surface heat flux Q in equations (3.10) and (3.12) reflects the penetration of radiation below the surface, as modelled by equation (3.4). Thus the diagnostic value of h will be dependent on the values of four tuning parameters: the C_i 's, the factor R and the vertical scale of penetration λ . Because Q is a relatively complex function of h , a solution for h from (3.4) and (3.13) is only possible by iterative techniques. An alternative method, which significantly reduces the computational effort, is to substitute the Obukhov length scale L for h in equation (3.4), and then solve for Q . This simplification is justified and will be utilized in the next sections, since the primary goal of this study is to examine the gross characteristics of the solution space.

Substituting (3.13) back into (3.7), the following expression for the vertically integrated dissipation is obtained:

$$D = m_1 \langle E \rangle^{3/2} = C_2 m_3 u_*^3 (1+2\Phi)/[2(1+C_2\Phi)]. \quad (3.16)$$

Physically, the dissipation must always be non-negative, which yields

$$1+2\Phi \geq 0$$

or

$$\Phi \geq -1/2. \quad (3.17)$$

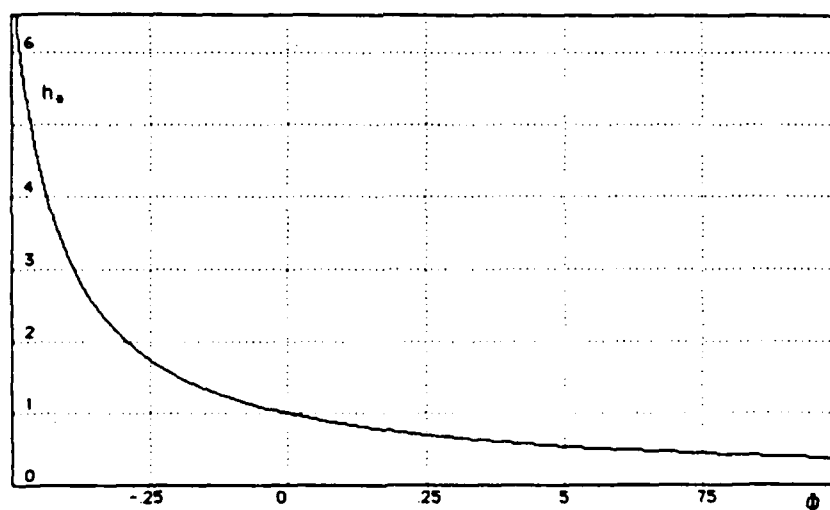


Fig. 3. The dimensionless depth scale h_* plotted against the rotation stress variable Φ .

For $\phi < -1/2$, and in absence of advection, no steady-state situation is possible and the mixed layer will continually entrain. Also, noting that, in equation (3.13), the denominator must be positive, the limiting case expressed by (3.17) suggests that $C_2 < 2$ for all situations (since C_2 is assumed to be a constant). Zeman and Tennekes (1975) obtained $m_2/m_1 \sim 1/2$, which gives $C_2 \sim 12/7$. Using the suggested value, a nondimensional mixed layer depth is given by (Fig. 3)

$$h_* = h / C_1 L = 1 / (1 + 12\phi / 7). \quad (3.18)$$

Note that to the limiting value $\phi = -1/2$ corresponds a theoretical maximum of $h_* = 7$.

IV. THE EQUILIBRIUM MIXED LAYER DEPTH IN THE TROPICAL ATLANTIC

A. THE BOUNDARY CONDITIONS

In the following sections, the method of application of the steady-state mixed layer model to an oceanic macro-scale domain is presented. The goal of this study is to gain insight into the relative importance of the physical mechanisms involved, as well as to identify the regions and the time of the year where the observed turbulent layer can be represented realistically by such a simple steady-state model. This goal is limited to some degree by the availability and suitability of experimental observations of the boundary conditions. Although a significant effort has been made in the last decade to obtain accurate and detailed measurements of the surface boundary conditions, such data are frequently confined to limited oceanic areas. The available climatological data for large oceanic areas are often unreliable, sparse and distributed irregularly, depending on the usual routes followed by mariners. Given these limitations, the tropical Atlantic Ocean is the best covered ocean basin.

Except for the observed surface wind-stress, where the digitized data of Hellerman and Rosenstein (1983) were used, all the other data were interpolated from climatological atlases. The area chosen was the tropical and equatorial Atlantic between 6 degrees south and 30 degrees north.

1. The Observed Mixed Layer Depth

The atlas of Robinson et al. (1979) was used to obtain the observed monthly values of the mean depths to the top of the thermocline for the

equatorial and tropical Atlantic. The top of the thermocline is therein defined as the depth at which the temperature is 1.1 degrees centigrade less than the surface temperature. Although this definition differs from the usual definition of "mixed layer depth" (the vertical extent of turbulent mixing), the difference should not be significant for the present study, provided density is mostly dependent upon temperature, and the boundary layer is well mixed. For the cases where the mixed layer mean temperature decreases significantly with depth, the above criterion might underestimate the vertical extent of mixing.

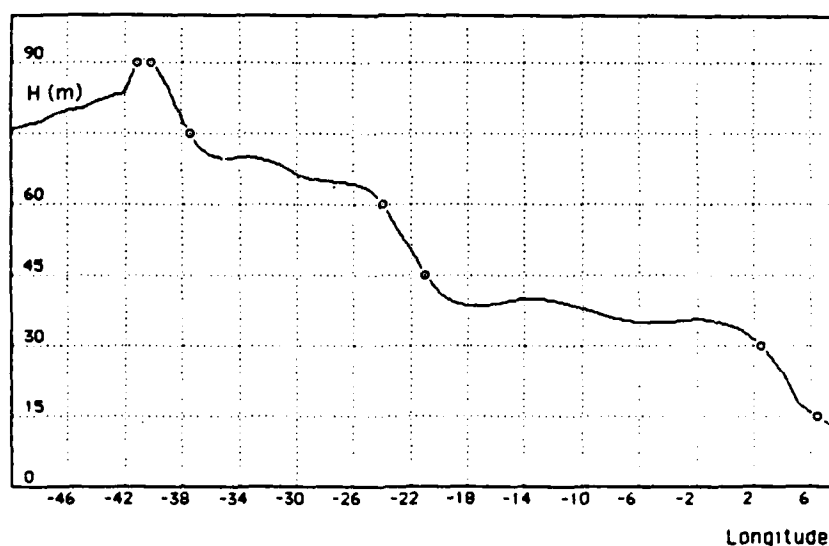


Fig. 4. Zonal variation of the mean mixed layer depth for the month of September (equator). The curve is the result of an adjusted cubic spline fit over the observed values, represented in the figure by circles.

Because the contours displayed in the atlas have a relatively large increment of 15 meters, a cubic spline fit was made for each parallel of latitude, and the resulting curve was further adjusted so that the interpolated values for each interval would lie between extremes. The resulting maximum graphical error is estimated to be ± 10 meters. No indication is given by the authors about the estimated errors for their analyzed depths.

Fig. 4 shows the zonal equatorial profile of the mean mixed layer depth for the month of September, as computed by the above technique.

2. The Surface Heat Flux

The heat budget atlas of Hastenrath and Lamb (1978) was used to provide best estimates of the net surface heat flux and the net surface solar irradiance for the area. For the assumptions made and the calculation details, the reader is referred to the introductory part of the atlas.

The contour interval for the surface heat flux is 40 W/m^2 , which constitutes a low resolution. In order to minimize the resulting errors, a cubic spline surface was first fitted over a grid of digitized values, and the resulting interpolated values were further adjusted for each parallel of latitude. Thus, for each interpolation interval, the calculated values would lie between extremes. The considerable effort required for this process is well justified because of the sensitivity of the diagnostic equations to small deviations in the values of Q_0 , specially when Q_0 is small.

The relative and absolute errors in the net surface heat flux, as indicated by the authors, are estimated at less than 10 and more than 20 W/m^2 , respectively. The absolute error in interpolated values is estimated to be less than 20 W/m^2 .

As an example, Fig. 7a shows the zonal equatorial profile of the mean surface heat flux for the month of September, as determined by the above technique.

3. The Surface Wind Stress

The surface wind stress data are those of Hellerman and Rosenstein (1983), for a mesh grid of 2 degrees of latitude by 2 degrees of longitude, which is suitable for our purpose. The two components are calculated by means of the bulk aerodynamic formulation:

$$\tau_x = \rho_a C_D U_x (U_x^2 + U_y^2)^{1/2} \quad (4.1)$$

and
$$\tau_y = \rho_a C_D U_y (U_x^2 + U_y^2)^{1/2}, \quad (4.2)$$

where U_x and U_y are the two components of the wind speed at 10 meters above the sea-surface. The drag coefficient, C_D , depends upon wind speed and stability, according to the formulation of Bunker (1976). The maximum standard error in the surface wind-stress values for the area considered is estimated to be less than 0.01 N/m².

The wind stress data are given for each odd whole degree of latitude and longitude, and in the present scheme we will be working with even parallels of latitude. Thus the original data had to be interpolated. The resulting interpolation errors are considered to be negligible for the purpose of the present study.

4. Steady-State versus Time-Dependent Solutions

Formally, a steady-state mixed layer model should only be applied to a real oceanic situation when entrainment has stopped and the top of the

thermocline has retreated to an equilibrium level, dependent on the balance between the downward surface heat flux and the surface wind-stress. On a seasonal time scale, i.e., neglecting daily variations, and for mid-latitudes, the above situation is expected to occur in spring and summer, when the mean downward surface heat flux is rising and the wind speed is decreasing. For the equatorial and tropical regions, however, this process is complicated, since the mean surface heat flux follows a complex annual variation, while the wind speed has a strong annual component.

For simplicity, the diagnostic mixed layer depth should be calculated for the same month throughout the chosen area, though the requirement of steadiness will not be satisfied in some regions. A logical and simple way to solve this problem is to plot the annual time series of the zonal profiles of the observed mixed layer depths for some parallels of latitude and choose the time of the year which best conforms to the condition of steadiness for all latitudes. Figure 5 shows these plots, as compiled and further interpolated from Robinson's atlas. The month of September was chosen as conforming best to these conditions. Except at the equator, where the top of the thermocline seems to be still deepening, the other latitudes show approximate steady-state situations, during September.

The analysis of Fig. 5a reveals a strong annual component of the equatorial mixed layer depth, which suggests the domination of the wind stress in determining the vertical extent of mixing. In Fig. 6, the annual time series of the net surface heat flux and the wind speed are shown. Indeed, a qualitative comparison of the contour lines of both figures (5a and 6) reveals a much stronger correlation between the mixed layer depth and the

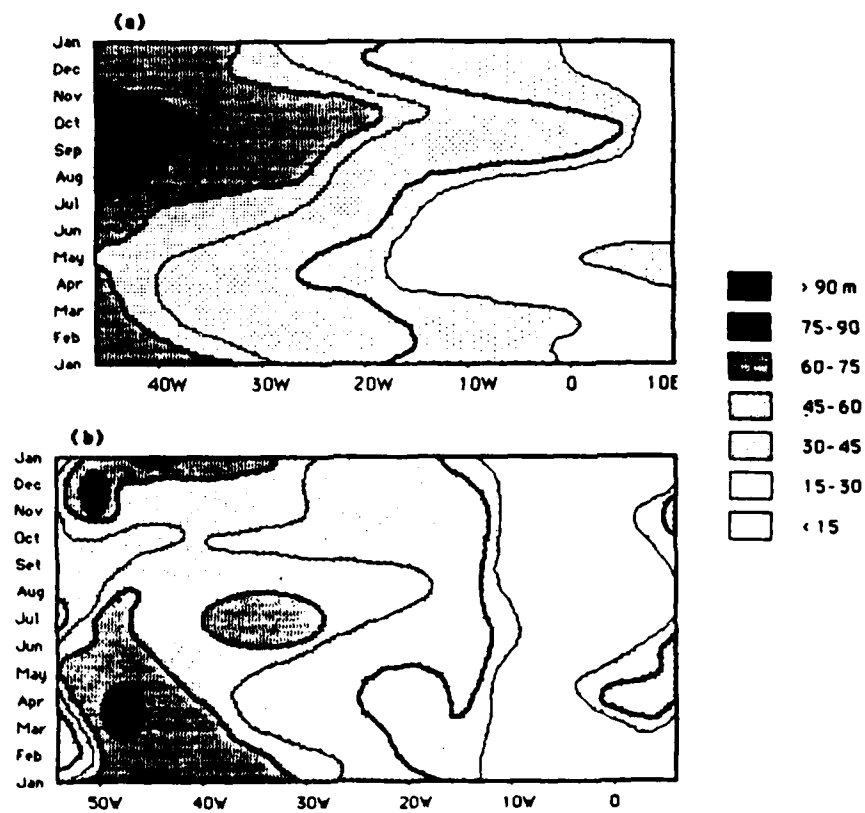


Fig. 5. Annual zonal variation of the mean mixed layer depth. (a) Equator. (b) 5 degrees north.

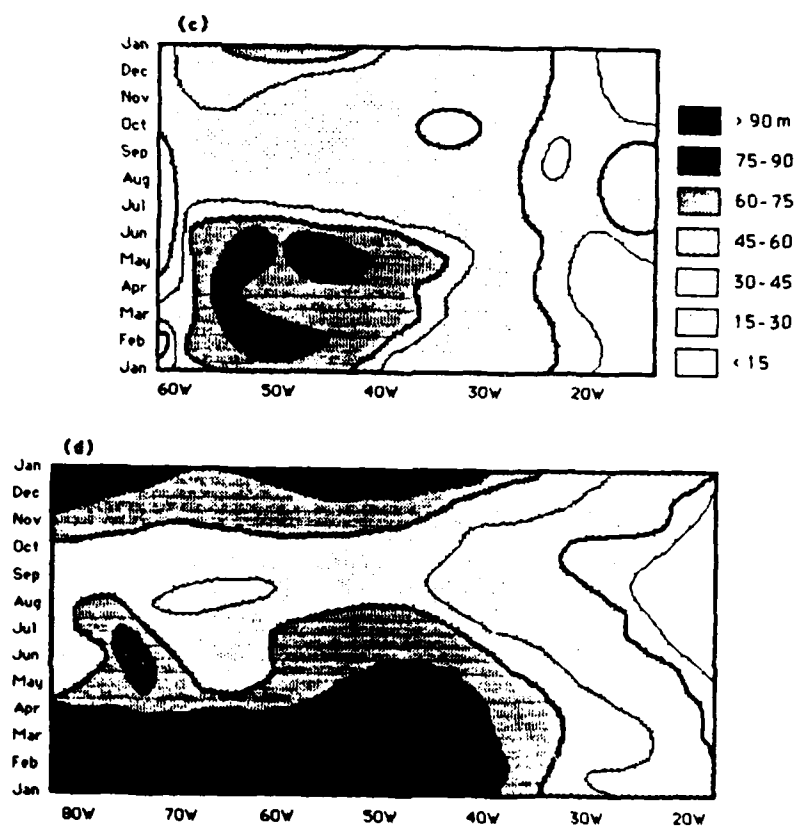


Fig. 5(cont.). Annual zonal variation of the mean mixed layer depth. (c) 10 degrees north. (d) 15 degrees north.

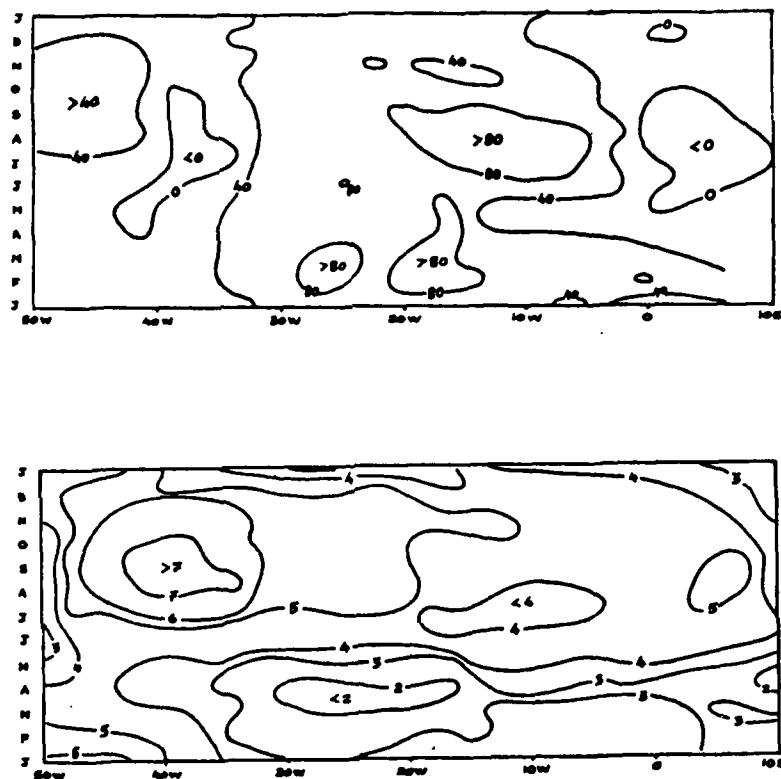


Fig. 6. (a) Annual zonal variation, in W/m^2 , of the net surface heat flux at the equator. (b) Annual zonal variation, in meters, of the wind speed at the equator.

wind speed than between the mixed layer depth and the surface heat flux. In particular, the wind speed maximum (August to October) and minimum (March to April), coincide well with the corresponding relative extremes in the mixed layer depth. Similar agreement is not apparent between the mixed layer depth and the surface heat flux, as so far as an equilibrium state is concerned.

On the other hand, one might expect the annual variation of the surface heat flux to show a marked response due to the annual variation of the Sun's declination, i.e., to show a strong biannual component. However, the exchange of heat between the ocean and the atmosphere is, in the equatorial and tropical regions, significantly influenced by other variables. These variables, such as cloudiness and precipitation, have seasonal variations which are more complex and difficult to explain.

During the months of May to September, another interesting feature in the eastern part of the Equator is the mixed layer depth minimum. This occurs when the surface heat flux is negative (upward). Without advection, an equilibrium situation is obviously precluded. Interestingly, the atlas of Robinson *et al.* (1979) shows that this is also a zone of strong equatorial upwelling and surface divergence. Thus, an advective mechanism may largely influence the dynamics of turbulent mixing for that region.

From the above discussion and also from the knowledge that the equatorial and tropical regions are zones of important oceanic heat divergence, it might be concluded that horizontal and vertical advection play an important role in determining the vertical extent of mixing at the equator. As lateral transport in the ocean diverts much of the heat exchanged with the

atmosphere, this effect would tend to spacially homogenize the surface heat flux available for the vertical turbulent processes. Thus, the seasonal variations of the mean mixed layer depth would primarily reflect the seasonal variations of the wind speed.

B. METHOD OF MODEL TUNING

The models described in sections II and III shall be applied to a set of some parallels of latitude in the tropical and equatorial Atlantic, from 6 degrees south to 30 degrees north. For each parallel, the spacing of calculated values will be 1 degree of longitude. The purpose of the following procedure is to identify the zones where the observed mixed layer is well represented by the above steady-state models, as well as to analyse the relative influence of the physical mechanisms discussed in section III: the penetration of radiation below the surface and the rotation stress mechanism. For each parallel of latitude, a zonal profile of the following nondimensional depth will be first calculated:

$$H_* = H (1 + C_2 \Phi) / L , \quad (4.3)$$

where H is the observed mixed layer depth and $C_2 = 12/7$. To calculate the Obukhov length scale L and the rotation stress variable Φ , the penetration parameters will be set to , respectively, $R=0.2$ and $\lambda = 6$ meters. Note that, for each longitude point, H_* is numerically equal to the constant C_1 . In the ideal case of a perfect agreement between the model's results and the observations, the resulting curve of H_* for each latitude would be a constant

of order 1. The departure of the calculated values from that ideal solution will constitute a method of identifying the zones where steadiness is not verified or advection plays an important role. For the situations where the surface heat flux is upward, i.e., where a one-dimensional equilibrium is not possible, H_* will be set to 0. The described procedure also makes possible the selection of the areas where the models will be applied. For these areas, the below defined diagnostic mixed layer depths will then be calculated:

(i) h_0 : the equilibrium mixed layer depth, assuming $R=0$, $C_2=0$. This corresponds to the steady-state Kraus and Turner diagnostic depth, where radiation is assumed to be totally absorbed at the surface.

(ii) h_1 : the equilibrium mixed layer depth, assuming $R=0.2$, $\lambda = 6\text{m}$, $C_2=0$. This is the same as h_0 , except that radiation is assumed to penetrate below the surface, according to the model given by equation (3.4).

(iii) h_2 : the equilibrium mixed layer depth, assuming $R=0.2$, $\lambda = 6\text{m}$ and $C_2 \neq 0$. Here, the rotation stress mechanism is also included, according to the formulation of Garwood *et al.* (1985a).

The pertinent equations are given in sections II and III, and the following constants are assumed:

$$\rho = 1025 \text{ Kg/m}^3$$

$$\rho_a = 1.2 \text{ Kg/m}^3$$

$$\alpha = 2 \times 10^{-4} \text{ C}^{-1}$$

$$C_p = 3890 \text{ J Kg}^{-1} \text{ C}^{-1}$$

$$g = 9.8 \text{ m/s}^2$$

$$\Omega = 7.29 \times 10^{-5} \text{ s}^{-1}.$$

For each of the above defined depths and for each latitude, the tuning constants C_1 and C_2 will be adjusted, so that the summation of the squares of the differences between the diagnostic mixed layer depths and the observed mixed layer depths is a minimum, and $C_1 \geq 0$ and $0 \leq C_2 \leq 2$. Following this tuning process, a standard deviation will be then computed, according to the definition:

$$s^2 = \sum_{i=1}^N (H_i - h_i)^2 / (N-1), \quad (4.4)$$

where the H_i 's are the observed mixed layer depths, the h_i 's are the diagnostic mixed layer depths and N is the number of longitude points. The standard deviations will serve as a quantitative verification of the models, the model assumptions, and the accuracy of the boundary conditions.

As discussed earlier, the rotation-stress variable Φ is required theoretically to be greater than $-1/2$, the value corresponding to a situation of zero dissipation. For that reason, Φ will be set equal to $-1/2$ whenever its calculated value is less than $-1/2$. During the month of September, this is likely to occur in the western Atlantic, where the zonal surface wind stress is large and the surface heat flux is small.

The selection of the factor R and the penetration depth λ is an imprecise process because of the paucity of data for the optical properties of the equatorial and tropical oceans. Although the choice here of values for R

and λ was based on a preliminary tuning of the model at a specific site, it is still somewhat arbitrary. Without a more complete data set, the inclusion of these parameters as spatially-varying tuning parameters does not seem justifiable at this time. Such a procedure would tend to mask the effects of other important physical mechanisms, such as horizontal and vertical advection. An alternative might be to define two different scales of penetration for the long and short-wave radiation, and then to use the experimental results of Paulson and Simpson (1977). However, this would also complicate the problem. Furthermore, Paulson and Simpson's data are valid only for a specific spatial and temporal situation in the North Pacific. In the absence of detailed measurements of the ocean's optical properties, there is no simple solution to this problem, and the results of the present work will be somewhat affected.

C. RESULTS

Appendix 1 shows the zonal variation of the nondimensional depth H_* for latitudes 0, 10, 20 and 30 degrees north. Only two particular cases, the equator and 10 degrees north, will be presented and discussed in the text.

1. Equator

Fig. 7 shows the equatorial boundary conditions: the surface heat flux Q_0 , the net surface solar irradiance Q_s , the total surface wind stress τ , and the zonal wind stress τ_x . Fig. 8a shows the zonal variation of the nondimensional depth H_* , computed using equation (4.3). It is apparent from this result that only a limited zone, between about 31 degrees west and 4 degrees west seems to be in a steady-state balance. For some of the remaining regions, the presence of an upward total surface heat flux precludes the possibility of an equilibrium, causing the top of the thermocline to continually entrain. We have previously suggested that the turbulent processes near the eastern boundary are likely to be dominated by equatorial upwelling, which can reduce significantly the vertical extent of mixing. The values from Fig. 7a seem to confirm this hypothesis, since the values of H_* are less than 1 near the coast. For the western region, other mechanisms might partially explain the departure of the model's results from the observations. The first of those is related to the strong wind-driven current near the coast of Brazil, the "Guiana current". This flow and the associated meridional variations in the surface heat flux might cause the local dynamics to be dominated by horizontal advection. A second possibly contributing factor is the influence of the Amazon River runoff. According to the data on the mean surface salinities in Robinson's atlas, this runoff extends to more

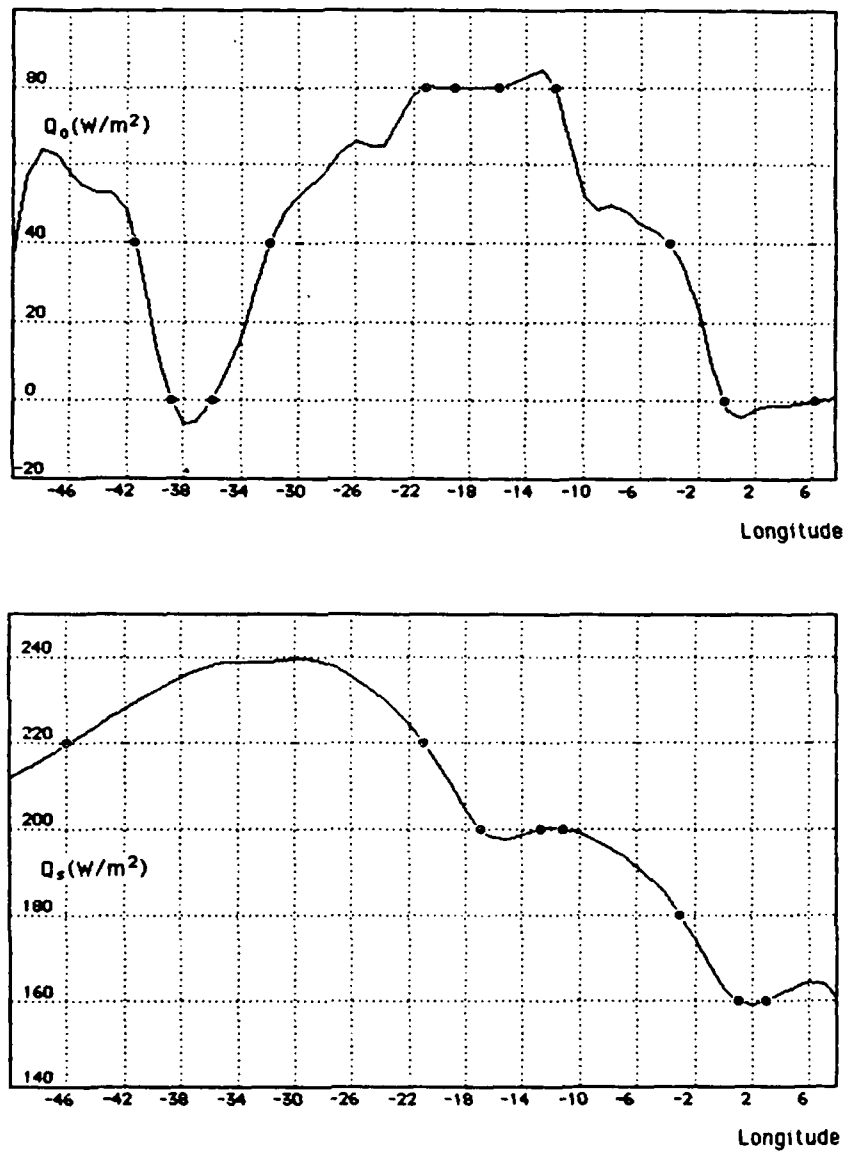


Fig. 7. Mean surface boundary conditions at the equator, during September. (a) Net downward surface heat flux. (b) Net downward surface solar irradiance.

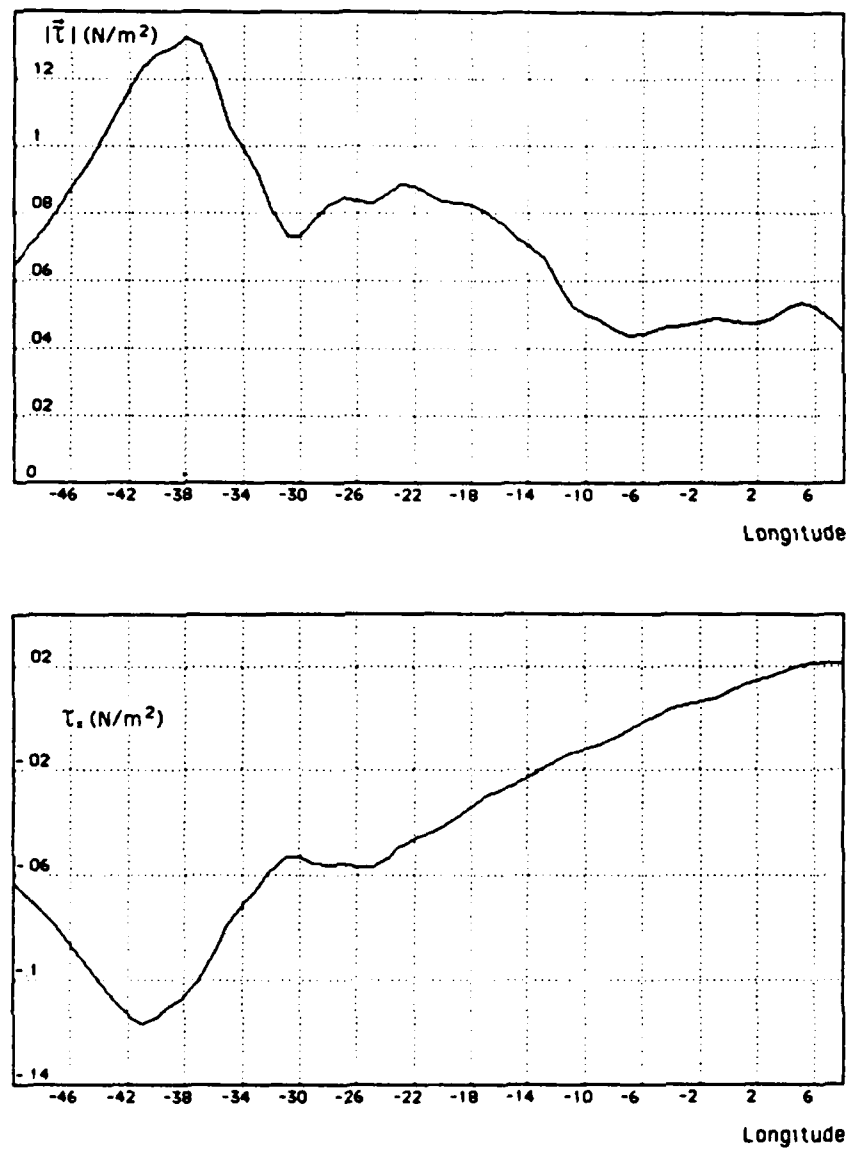


Fig. 7(cont.). Mean surface boundary conditions at the equator, during September. (c) Total surface wind stress. (d) Zonal surface wind stress.

than 300 nautical miles eastward from the coast and it affects the upper few tens of meters of the water column. As examined by Garvine (1984), an advected shallow plume of buoyant water can decrease the mixed layer depth. Also, since the water advected from the Amazon is more turbid than the average sea water, the value chosen for the penetration scale λ is probably too large for the region, causing the model to overestimate the mixed layer depth. Fig. 7a shows precisely this effect : approaching the western boundary, H_* falls markedly to about 0.4.

For the equatorial region between 31 degrees west and 4 degrees west, the diagnostic values were calculated for the mixed layer depths scales h_0 , h_1 and h_2 . The results were compared with the observed mixed layer depths. Fig. 8 shows the zonal profiles obtained for each of the defined scales. The vertical bars represent the effect of varying Q_0 by $\pm 10 \text{ W/m}^2$, which indicates how sensitive the model is to moderate errors or variations in the heat flux data. The comparison of Figures 7a and 8 also shows that h_2 is significantly more sensitive to variations in Q_0 than are the other depth scales, especially when Q_0 is small. In determining a best fit for h_0 and h_1 , the corresponding standard deviations were $s_0 = 5.4$ meters and $s_1 = 6.2$ meters. These optimized values were obtained with $C_1 = 1.3$ and $C_1 = 1.0$, for h_0 and h_1 , respectively.

Fig. 9 illustrates the tuning process of C_1 and C_2 , in computing the zonal variation of the depth scale h_2 . Displayed here are isopleths, in m^2 , of the sums of the squares of the differences between the diagnostic and the observed depths, as a function of C_1 and C_2 values. For each grid point of C_1 and C_2 values, a zonal profile of the diagnostic depth h_2 was calculated,

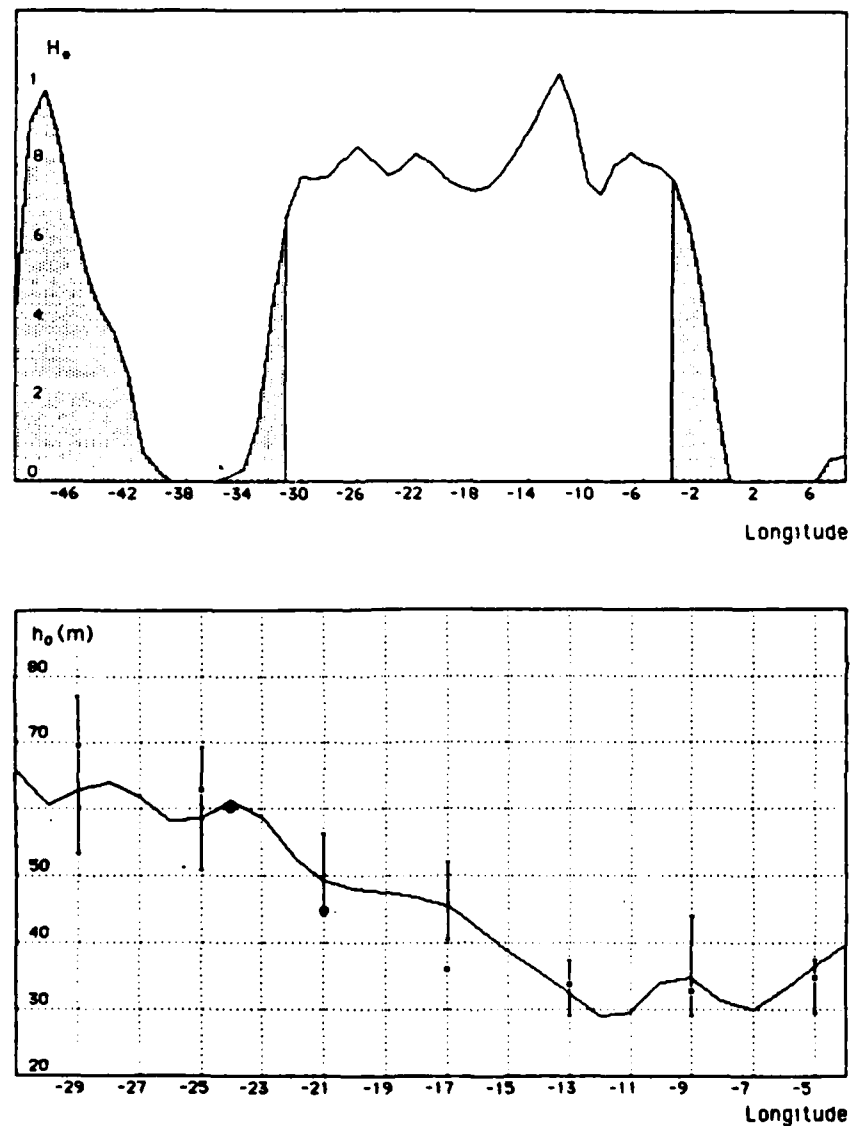


Fig. 8. Model results for the equator. (a) Zonal variation of the nondimensional mixed layer depth H_* . (b) Zonal variation of the Kraus and Turner diagnostic mixed layer depth h_0 . The circles represent observed values, while the small squares represent interpolated values. The vertical bars show the effect of varying the surface heat flux Q_0 by $\pm 10 \text{ W/m}^2$. The shaded areas in (a) correspond to the zones where a one-dimensional, steady-state balance is assumed impossible.

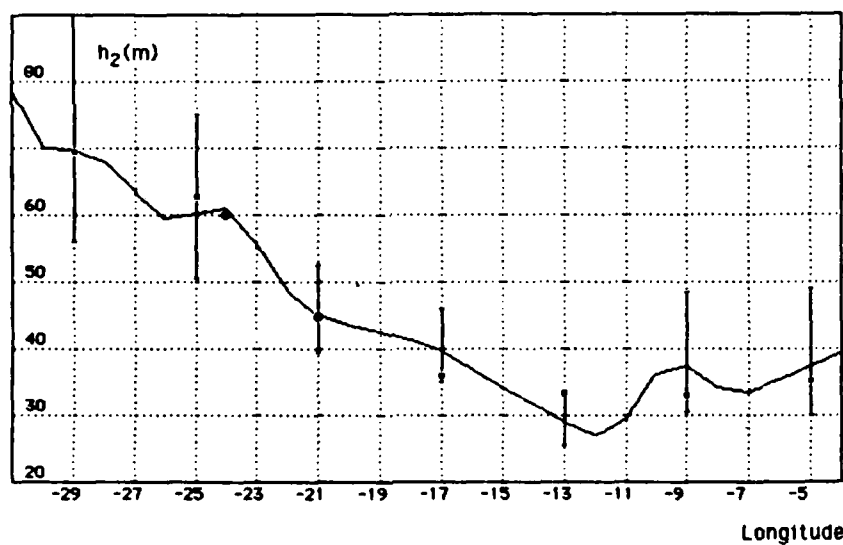
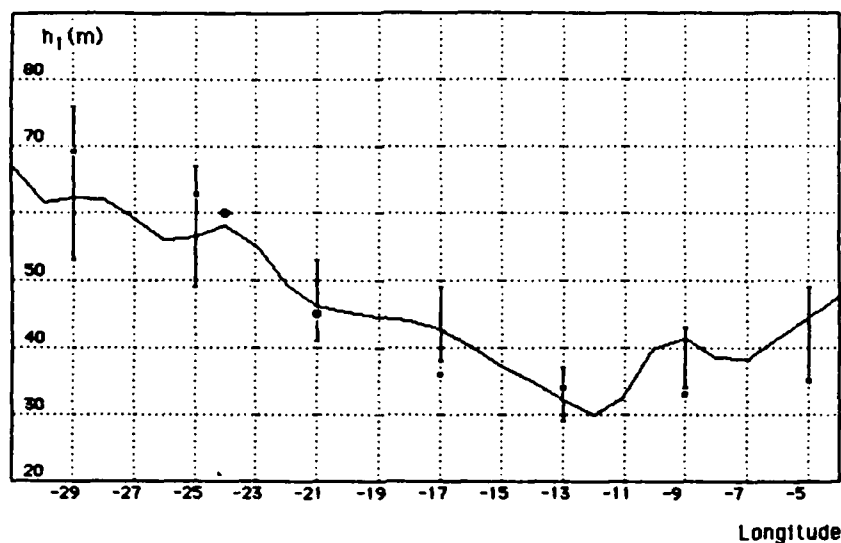


Fig. 8(cont.). Model results for the equator. (c) Zonal variation of the Kraus and Turner diagnostic mixed layer depth h_1 . (d) Zonal variation of the Garwood diagnostic mixed layer depth h_2 . The circles represent observed values, while the small squares represent interpolated values. The vertical bars show the effect of varying the surface heat flux Q_0 by $\pm 10 \text{ W/m}^2$.

as well as the zonal summation of the squares of the differences between those depths and the observed mixed layer depths. The arrows in Fig.9 indicate the optimal values of the constants, corresponding to a minimum standard deviation $s_2 = 3.3$ meters.

There are some interesting features to be noted in the results:

(i) There is no quantitative improvement in the quality of the results for the Kraus and Turner model (h_0) when the effect of the penetrating radiation is included (h_1). This is explained by the fact that the surface heat flux is relatively large in that region, and the vertical scale λ of penetration is much less than the computed Obukhov length scale.

(ii) The zonal variation of the mixed layer depth near the western limit is better represented when the rotation stress mechanism is included (h_2). In that region, the zonal wind stress has relatively large negative values, which causes Φ to also have relatively large negative values.

(iii) The model seems much more sensitive to the value of C_1 than to the value of C_2 . Fig. 9 shows a relatively large zone, between $C_2=1.2$ and $C_2=1.6$ where the standard deviation remains practically constant. This fact, associated with the similarity of the results between h_0 and h_1 , might indicate that the effect of the rotation stress mechanism is small, for the region taken as a whole.

In general, the revised model shows a remarkably good agreement with the observations. However, and because the Kraus and Turner h_0 's are already, *per se*, in good agreement with the observed values, the results

are not conclusive concerning the importance of the penetrating radiation and the rotation stress mechanism. The eastern part of the equator, where the observed zonal wind stress is positive, would constitute a suitable domain to further test the significance of the rotation stress mechanism. There, the diagnostic depths h_2 would be larger than the Kraus and Turner depths h_0 and h_1 . However, as we have seen, other mechanisms appear to affect the dynamics of mixing in the region, and will need to be included in such a test.

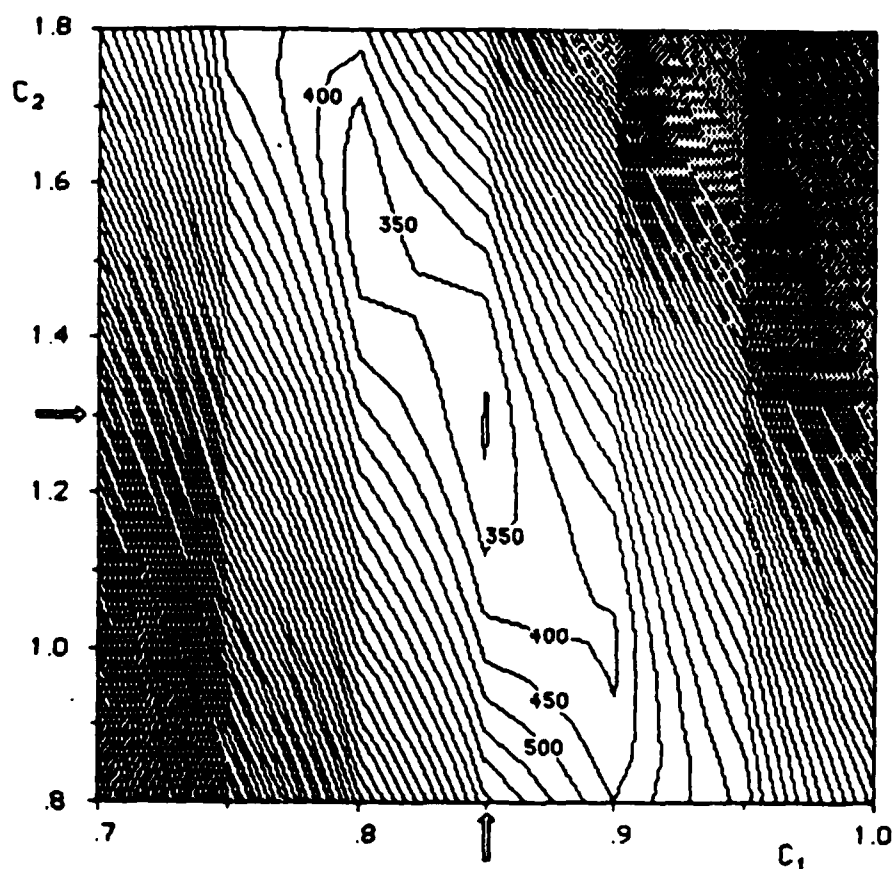


Fig. 9. Variation of the sum of the squares of the differences, in m^2 , between the observed equatorial mixed layer depths H and the diagnostic mixed layer depths h_2 with the tuning parameters C_1 and C_2 .

2. 10 degrees North

Fig. 10 shows the mean boundary conditions for 10 degrees north during the month of September. In Fig. 11a, the zonal variation of the nondimensional depth H_* is displayed. This figure shows that the zone which seems to be in a steady-state balance (between about 38 degrees west and 17 degrees west) is considerably smaller than the corresponding zone for the equator. Although the surface heat flux is always positive for the entire domain, the values are usually smaller than at the equator. When the effect of the penetration of radiation is included, the result is to further reduce the effective heat flux at the surface, as defined by equation (3.4). This effect reduces buoyant damping and precludes the possibility of an equilibrium for a larger area. Although unsteadiness may partially account for these results, advection seems to be a more plausible explanation for the regions where the effective heat flux is positive, since H_* is always less than 1. A meridional gradient is present in the surface heat flux because of the strong wind-driven current in the western part of the tropical Atlantic, and this effect might cause buoyant water to be advected northward, reducing the vertical extent of mixing. The variation of H_* near the eastern boundary is more difficult to explain. From about 18 degrees west, where it has a value of 1, H_* continues to increase eastward, which indicates that the observed depth becomes larger than the diagnostic depth h_2 . The analysis of the temperature distribution in the atlas of Robinson *et al.* (1979) shows that this is a region of particularly strong coastal upwelling. However, positive vertical advection can only reduce the depth of the turbulent boundary layer, as

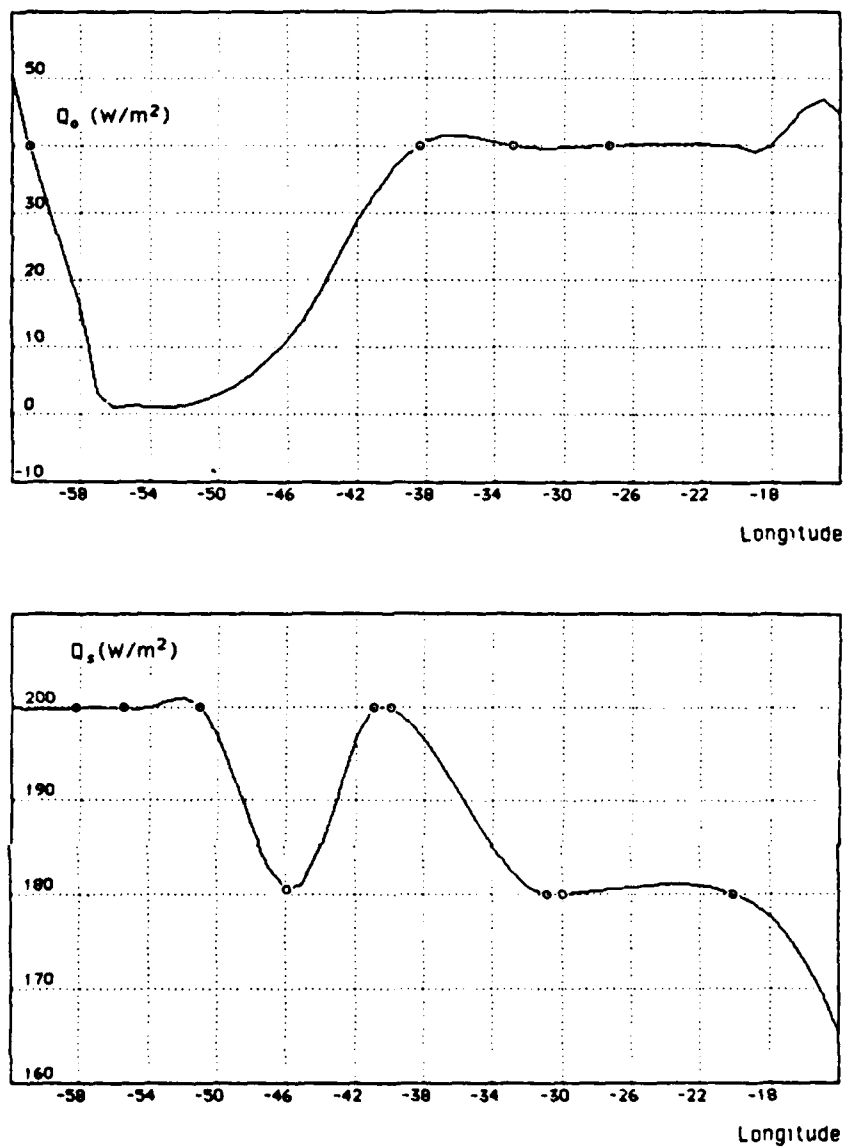


Fig. 10. Mean surface boundary conditions at 10 degrees north, during September. (a) Net downward surface heat flux. (b) Net downward surface solar irradiance.

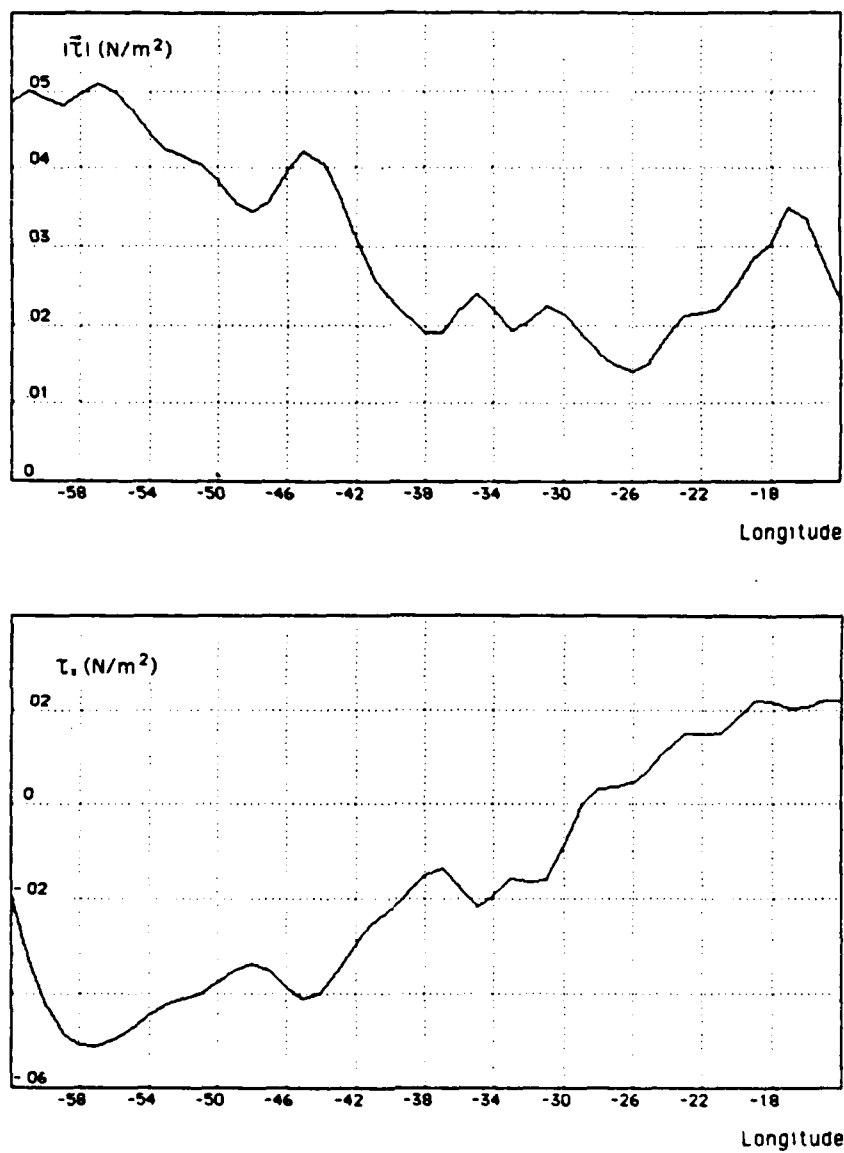


Fig. 10(cont). Mean surface boundary conditions at 10 degrees north, during September. (c) Total surface wind stress. (d) Zonal surface wind stress.

stated by Garwood *et al.* (1985b). Thus, this mechanism cannot be responsible for the difference.

The diagnostic depths h_0 , h_1 and h_2 were calculated for the region between 38 degrees west and 17 degrees west. Fig. 11 shows their zonal variations. The vertical bars represent the effect of varying Q_0 by $\pm 5 \text{ W/m}^2$, from which it can be concluded that the model is much more sensitive here to small variations in the heat flux than it was for the equator, especially when the penetration of radiation effect is included. This is explained by the already discussed fact that the surface heat flux at 10 degrees north is significantly smaller than it is at the equator. In some areas, particularly in the western half of the domain, the sensitivity is so large that the resulting depths vary by a factor of three when those effects are considered. Considering that the relative errors in the surface heat flux data, as estimated by Hastenrath and Lamb (1978), are less than 10 W/m^2 , only a qualitative interpretation of the results for this latitude should be made.

For each of the diagnostic scales h_0 , h_1 and h_2 , the optimized tuning constants and the corresponding standard deviations have the following values:

$$h_0 : C_1 = 2.6, C_2 = 0.0, s = 11.8 \text{ m}$$

$$h_1 : C_1 = 0.8, C_2 = 0.0, s = 7.1 \text{ m}$$

$$h_2 : C_1 = 0.8, C_2 = 0.7, s = 5.9 \text{ m}.$$

A significant improvement in the quantitative quality of the results is apparent, when the penetration effect is included (h_1). Note that the optimum

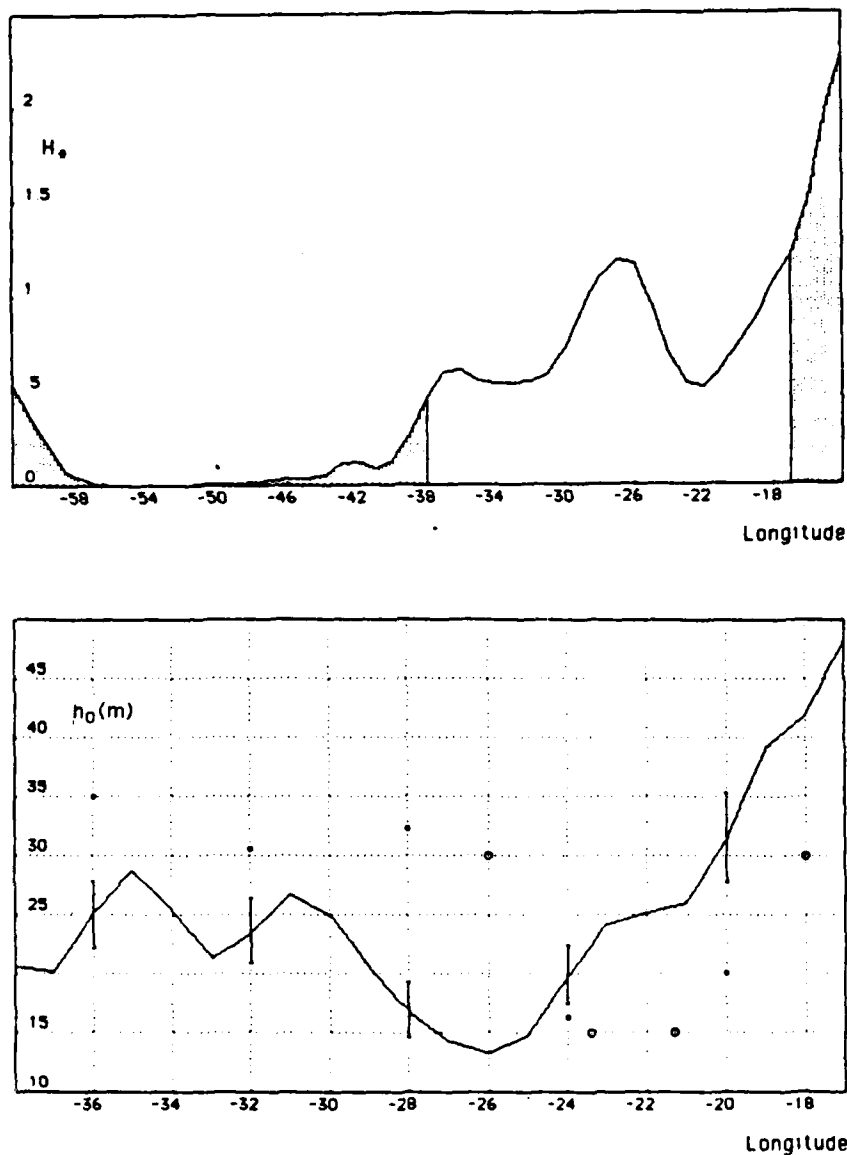


Fig. 11. Model results for 10 degrees north. (a) Zonal variation of the nondimensional mixed layer depth H_* . (b) Zonal variation of the Kraus and Turner diagnostic mixed layer depth h_0 . The circles represent observed values, while the small squares represent interpolated values. The vertical bars show the effect of varying the surface heat flux Q_0 by $\pm 5 \text{ W/m}^2$. The shaded areas in (a) correspond to the zones where a one-dimensional, steady-state balance is assumed impossible.

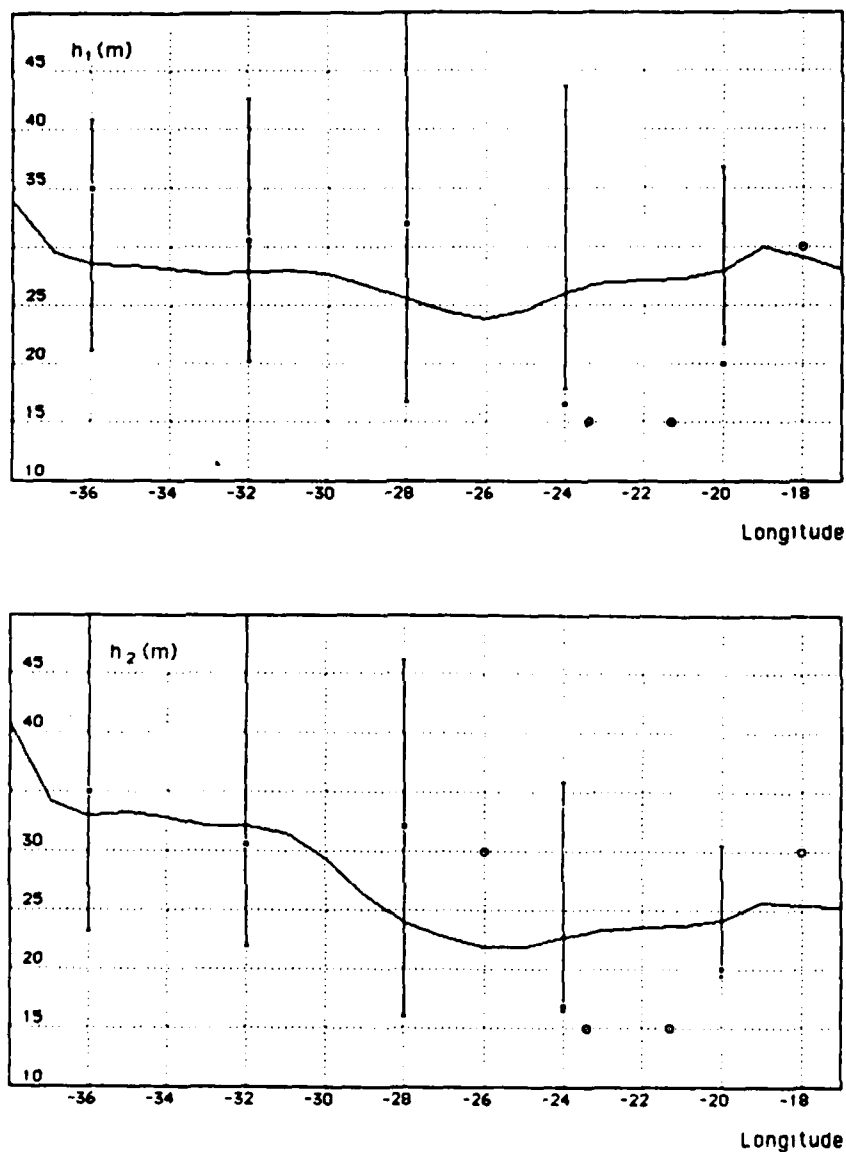


Fig. 11(cont). Model results for 10 degrees north. (c) Zonal variation of the Kraus and Turner diagnostic mixed layer depth h_1 . (d) Zonal variation of the Garwood diagnostic mixed layer depth h_2 . The circles represent observed values, while the small squares represent interpolated values. The vertical bars show the effect of varying the surface heat flux Q_0 by $\pm 5 \text{ W/m}^2$.

tuned value of C_1 was reduced from 2.6 to a more plausible 0.8, which approaches the value found for the equator. In general, the inclusion of the penetration effect tended to homogenize the diagnostic mixed layer depth field. This caused a better agreement between the results and the observations, particularly near the extremes of the longitudinal interval. As expected from the analysis of the boundary conditions for the zonal wind stress, the western part of the domain is better represented when the rotation stress mechanism is included. Also, a small improvement is observed near 22 degrees west, where the observed mixed layer depth has a minimum. This is explained by the zonal wind stress being positive in that region. When the eastern boundary is approached, τ_x becomes more and more positive, causing the diagnosed value for h_2 to be less than the observed value.

Fig. 11 illustrates the tuning process for h_2 . Again, the contour lines, in m^2 , of the sums of the squares of the differences between the diagnostic and the observed depths, are displayed as a function of C_1 and C_2 . The optimal value of $C_1 = 0.8$ has not changed with the inclusion of the rotation stress mechanism. This tends to verify the merits of the procedure, in the sense that no other physical mechanisms, absent from the model's formulation, are being compensated for. On the other hand, although Fig. 11 shows that the model is still more sensitive to variations in C_1 than to variations in C_2 , the optimal value of C_2 is much better defined here than at the equator. Also, this relative sensitivity seems to verify the importance of the rotation effect.

Although a much better representation of the mixed layer depth field was obtained with the revised model at 10 degrees north, this verification is limited by the uncertainty in the boundary conditions. As we have already noted, the model is so sensitive to small variations in the heat flux data, that no detailed interpretation of the results is justifiable.

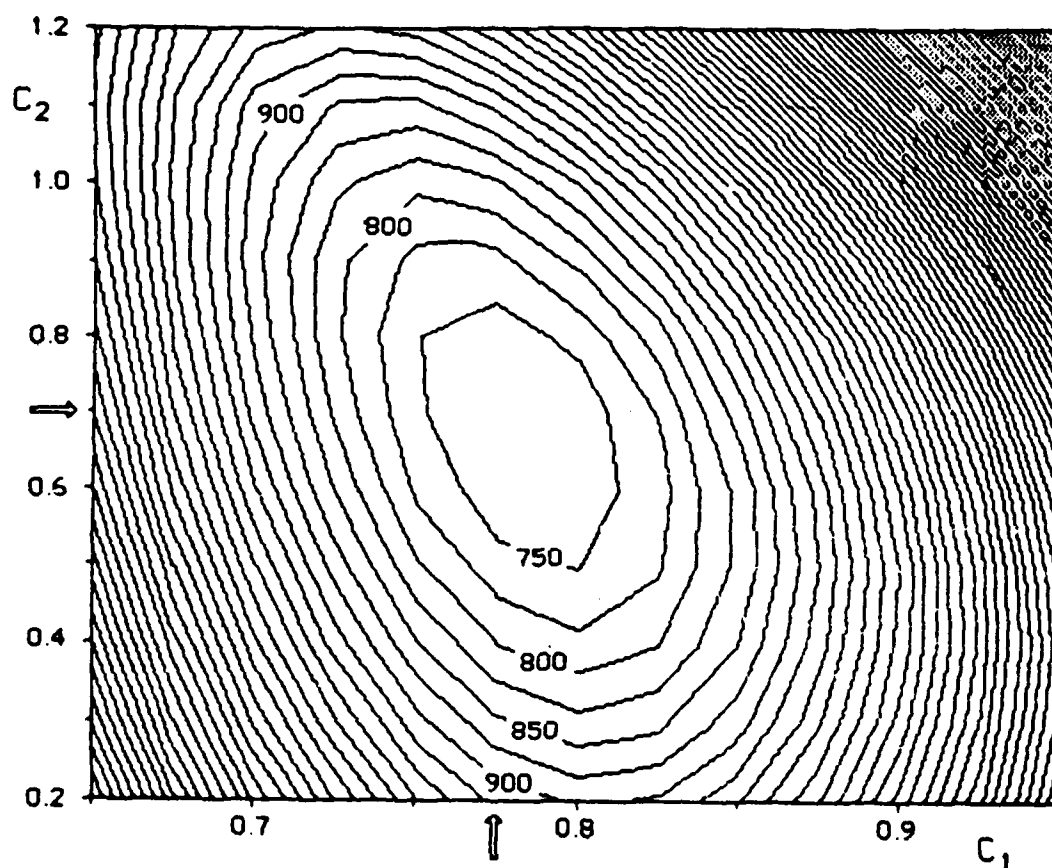


Fig. 12. Variation of the sum of the squares of the differences, in m^2 , between the observed mixed layer depths H and the diagnostic mixed layer depths h_2 with the tuning parameters C_1 and C_2 (10 degrees north).

V. CONCLUSIONS

Starting with the theoretical frame work of the one-dimensional, steady-state Kraus and Turner (1967) model for the surface ocean boundary layer, a revised theory was presented. This new theory includes the effect of the penetrating radiation below the surface on the buoyancy flux, as well as the rotation stress mechanism examined by Garwood (1985a,b). In the presence of a downward surface heat flux and a surface wind stress, the penetration of radiation will tend to reduce the buoyant damping of turbulence, enhancing vertical mixing. The rotation stress mechanism, driven by the interaction between the meridional component of the planetary rotation Ω_y and the zonal wind stress τ_x , predicts the equilibrium mixed layer depth to increase when τ_x is negative (westward) and to decrease when τ_x is positive (eastward).

To test its response, and to gain insight into the relative importance of the physical mechanisms involved, the revised model was applied to a set of boundary conditions in the tropical Atlantic. Except for the surface wind stress, where digitized values were used, the other boundary and oceanic conditions (observed mixed layer depth, surface heat flux and surface downward solar irradiance) were interpolated from low-resolution climatological atlases. Since the model is particularly sensitive to small variations in the heat flux data, the quality of the results is considered to have been somewhat affected by the amount of uncertainty in the boundary conditions. Also, in the absence of detailed measurements of the optical properties of the tropical oceans, the values of the penetration parameters λ

and R were assumed to be constant over the whole domain. Given these limitations, no detailed interpretation of the results is appropriate here.

In general, the response of the revised model compares favorably with the observations. The improvement of the results when the two new mechanisms are included is very significant, particularly at 10 degrees north. This was expected, in so far as the penetration effect is concerned, since at 10 degrees north the mixed layer is relatively shallower than at the equator, and the downward surface heat flux is generally smaller. For this latitude, an important result which seems to support the need to include the rotation stress formulation is that the optimal value of the constant C_1 remains constant when that process is included in the tuning of the model.

In a recent paper, Garwood *et al.* (1985b) examined the zonal dependence of the climatological mixed layer depth in the near-equatorial Pacific and concluded that the rotation stress mechanism is a plausible explanation for the deep mixing in the central equatorial Pacific. Although that feature is not so pronounced in the tropical and near-equatorial Atlantic, the results obtained here seem to support the same conclusion, especially in its western part. On the other hand, the tropical Atlantic is a relatively smaller ocean basin, and the influence of coastal physical processes, like coastal upwelling, are more likely to influence significantly the dynamics of the boundary layer. Indeed, this effect is apparent from the results, since only the central part of the domain seems to be in a one-dimensional equilibrium state. Also, the sensitivity of the model to small variations in the surface heat flux shows that this equilibrium state is, as it is in the tropical Pacific, a delicate one.

The choice of the tropical Atlantic as a domain for application of the model was primarily motivated by the existence of a suitable set of surface boundary condition data. Future research on the subject should extend the domain to the non-tropical regions and should include unsteadiness and advection. Although the model derived in this paper is a simplistic one-dimensional representation of a complex phenomenon, and the quality of the results were probably affected by the lack of detail of the available data, it is concluded here that the physical mechanisms of rotation stress and penetration of radiation are important in determining a steady-state equilibrium depth of turbulent mixing for the tropical Atlantic.

LIST OF REFERENCES

- Garvine, R.W., 1984 : Radial spreading of buoyant, surface plumes in coastal waters. *Journal of Geophysical Research*, **89**, 1989-1996.
- Garwood, R.W., 1977 : An oceanic mixed layer model capable of simulating cyclic states. *Journal of Physical Oceanography*, **7**, 455-468.
- Garwood, R.W., P.C. Gallacher and P. Muller, 1985a : Wind direction and equilibrium mixed layer depth : General theory. *Journal of Physical Oceanography*, in press.
- Garwood, R.W., P. Muller and P.C. Gallacher, 1985b : Wind direction and equilibrium mixed layer depth in the Tropical Pacific Ocean. *Journal of Physical Oceanography*, in press.
- Hastenrath, S., and P.J. Lamb, 1978: *Heat Budget Atlas of the Tropical Atlantic and Eastern Pacific Oceans*. The University of Wisconsin Press.
- Hellerman, S., and M. Rosenstein, 1983 : Normal monthly wind stress over the world ocean with error estimates. *Journal of Physical Oceanography*, **13**, 1093-1104.
- Kraus, E.B., and J.S. Turner, 1967 : A one-dimensional model of the seasonal thermocline, II: The general theory and its consequences. *Tellus*, **19**, 98-105.
- Paulson, C.A., and J.J. Simpson, 1977 : Irradiance measurements in the upper ocean. *Journal of Physical Oceanography*, **7**, 952-956.
- Robinson, M.K., R.A. Bauer and E.H. Schroeder, 1979 : *Atlas of North Atlantic-Indian Ocean Monthly Mean Temperatures and Mean Salinities of the Surface Layer*. Naval Oceanographic Office.
- Rotta, J.C., 1951 : Statistische Theorie nichthomogener Turbulenz. *Z. Phys.*, **129**, 547-572.
- Simpson, J.J., and T.D. Dickey, 1981 : The relationship between downward irradiance and upper ocean structure. *Journal of Physical Oceanography*, **11**, 309-323.

Tennekes, H., and J.L. Lumley, 1972 : *A First Course in Turbulence*. The MIT Press, Cambridge, Massachusetts, 300 pp.

APPENDIX A - MODEL OUTPUT

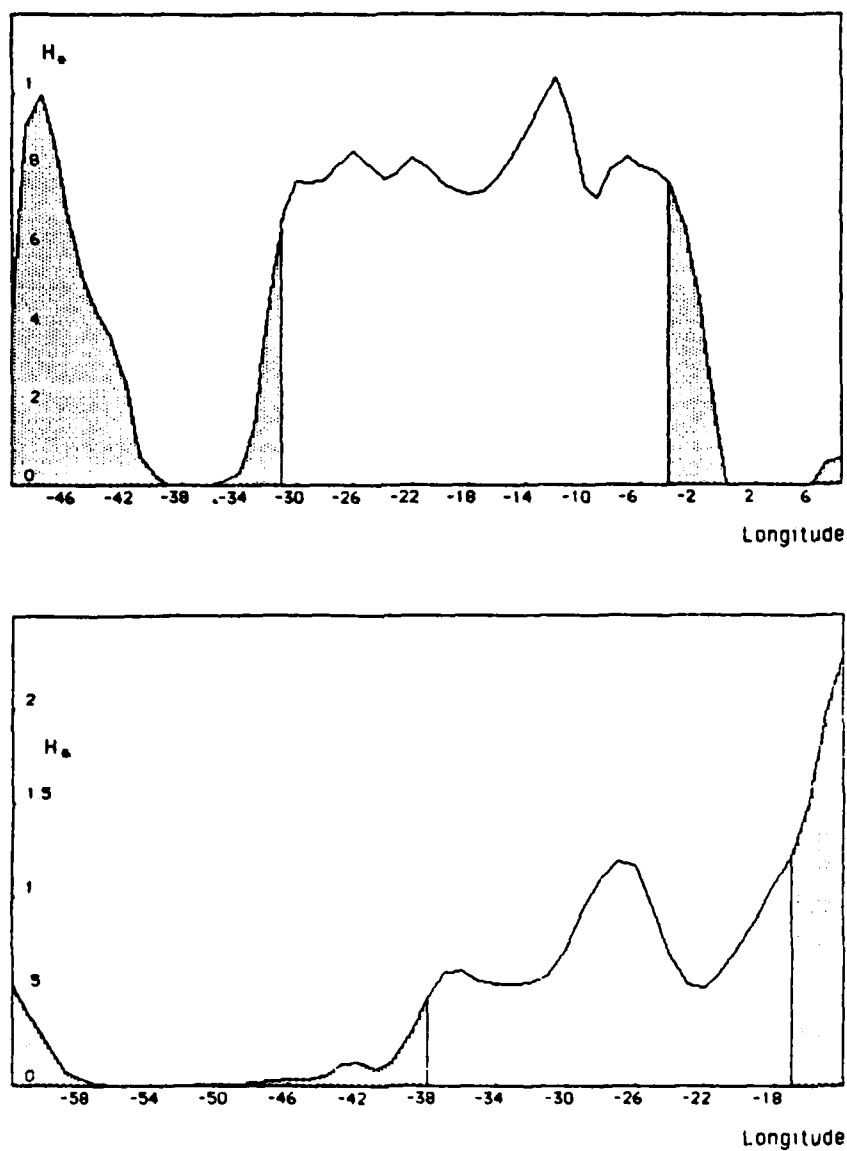


Fig. 13. Zonal variation of the nondimensional mixed layer depth H_* . Top : equator. Bottom : 10 degrees north. The shaded areas correspond to the zones where a one-dimensional, steady-state balance is assumed impossible.

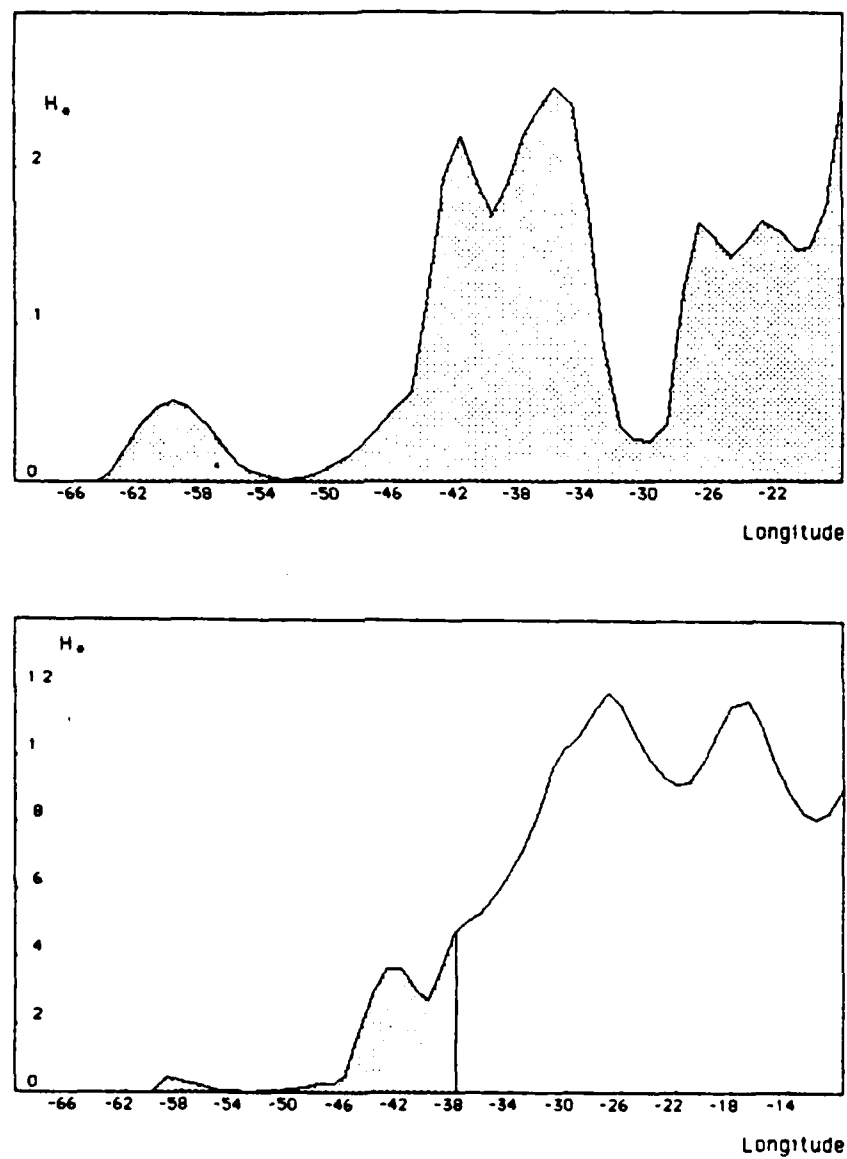


Fig. 14. Zonal variation of the nondimensional mixed layer depth H_* . Top : 20 degrees north. Bottom : 30 degrees north. The shaded areas correspond to the zones where a one-dimensional, steady-state balance is assumed impossible.

APPENDIX B - COMPUTER PROGRAMS

Program depth - calculates the steady-state mixed layer depth variation for a given parallel of latitude.
Joaquim Filipe Gaspar - April 1985 - **Naval Postgraduate School.**

```
DEFINT i-k,n
DIM long(200),Qo(200),Qs(200),tau(200),taux(200),depth(200),h(200)
```

```
***** Variables *****
lat - latitude in degrees ; long - longitude in degrees
Qo - surface heat flux in  $W/m^2$  ; Qs - surface solar irradiance in  $W/m^2$ 
Q - effective heat flux in  $W/m^2$ 
tau - total wind stress in  $N/m^2$  ; taux - zonal wind stress in  $N/m^2$ 
depth - observed mixed layer depth in meters
h - diagnostic mixed layer depth in meters
L - Obukhov length scale in meters
Fi - rotation stress parameter
R,lb - radiation penetration parameters
c1,c2 - model tuning parameters.
*****
```

Inputdata:

```
INPUT "Enter latitude "; lat: lat$=STR$(lat)
f1$="sh"+lat$ : OPEN "in",#1,f1$
f2$="qs"+lat$ : OPEN "in",#2,f2$
f3$="tau"+lat$ : OPEN "in",#3,f3$
f4$="taux"+lat$ : OPEN "in",#4,f4$
f5$="mld"+lat$ : OPEN "in",#5,f5$
```

n=0

```
WHILE NOT EOF(1)
```

```
  n=n+1
```

```
  INPUT#1,long(n),Qo(n)
```

```
  INPUT#2,lq,Qs(n)
```

```
  INPUT#3,lq,tau(n)
```

```
  INPUT#4,lq,taux(n)
```

```
  INPUT#5,lq,depth(n)
```

```
WEND
```

```
CLOSE
```

Inputparameters:

```
PRINT "Longitude limits in files are "; long(1),long(n)
INPUT "Enter new longitude limits "; long0,long1
IF long0<long(1) OR long1>long(n) THEN Inputparameters
INPUT "Enter value of C1 "; c1
INPUT "Enter value of C2 "; c2
10 INPUT "Enter value of R "; R : IF R<0 OR R>1 THEN 10
20 INPUT "Enter value of lambda "; lb : IF lb<=0 THEN 20
```

Functions:

```
DEF FNL(tau,Q)=124078!*tau^1.5/Q
DEF FNQ(Qo,Qs,L)=Qo-R*Qs*(2*lb/L-(1+2*lb/L)*EXP(-L/lb))
DEF FNFi(taux,Q)=144.6*taux*COS(lat/57.2958)/Q
```

Calculate:

```
sum=0
FOR i=1 TO n
  IF long(i)<long0 OR long(i)>long1 THEN 30
  IF Qo(i)<=0 THEN h(i)=0 : c$="*": GOTO display
  L=FNL(tau(i),Qo(i))
  Q=FNQ(Qo(i),Qs(i),L):IF Q<=0 THEN h(i)=0:c$="*":GOTO display
  L=FNL(tau(i),Q)
  Fi=FNFi(taux(i),Q) : IF Fi<-.5 THEN Fi=-.5
  h(i)=c1*L/(1+c2*Fi)
  sum=sum+(depth(i)-h(i))^2
  c$=" "
  display:
  PRINT long(i);c$,h(i)
30 NEXT i
PRINT "Sum : "; sum
```

Choose:

```
INPUT " Save results(1),New files(2), new parameters(3), Quit(4) "; o
ON o GOTO Saveresults,Inputdata, Inputparameters,quit
```

Saveresults:

```
INPUT "Enter name of output file "; fo$
OPEN "out",#5,fo$
FOR i=1 TO n
  WRITE#5,long(i),h(i)
NEXT i
CLOSE
GOTO Choose
```

Quit:

```
END
```

Program Spline - fits a cubic spline over a set of (x,y) points.
Joaquim Filipe Gaspar - January 1985 - **Naval Postgraduate School**

```
DIM x(200),y(200),a(200,4),s(200) : DEFINT i,j,n,e
DIM a0(200),a1(200),a2(200),a3(200)
```

Enterdata:

```
INPUT "Read disk file(d) or enter data from keyboard(k) "; a$
IF a$="k" THEN key ELSE IF a$="d" THEN disk ELSE Enterdata
```

disk:

```
INPUT "Enter name of file to fit "; f$
OPEN "in",#1,f$
n=1
WHILE NOT EOF(1)
    INPUT#1,x(n),y(n)
    n=n+1
WEND
CLOSE#1
n=n-1 : GOTO Endc
```

key:

```
INPUT "Enter number of points "; n
FOR i=1 TO n : PRINT i, : INPUT x(i),y(i) : NEXT i
```

Endc:

```
INPUT "Enter end condition (1,2 or 3) "; endcond
```

```
nm2=n-2 : nm1=n-1
dx1=x(2)-x(1) : dy1=(y(2)-y(1))/dx1*6
```

defmatrix:

```
FOR i=1 TO nm2
    dx2=x(i+2)-x(i+1)
    dy2=(y(i+2)-y(i+1))/dx2*6
    a(1,1)=dx1 : a(1,2)=2*(dx1+dx2)
    a(i,3)=dx2 : a(i,4)=dy2-dy1
    dx1=dx2 : dy1=dy2
NEXT i
```

```
ON endcond GOTO solve,end2,end3
```

end2:

```
a(1,2)=a(1,2)+x(2)-x(1)
a(nm2,2)=a(nm2,2)+x(n)-x(nm1)
GOTO solve
```

```

end3:
  dx1=x(2)-x(1) : dx2=x(3)-x(2)
  a(1,2)=(dx1+dx2)*(dx1+2*dx2)/dx2
  a(1,3)=(dx2*dx2-dx1*dx1)/dx2
  dxn2=x(nm1)-x(nm2) : dxn1=x(n)-x(nm1)
  a(nm2,1)=(dxn2*dxn2-dxn1*dxn1)/dxn2
  a(nm2,2)=(dxn1+dxn2)*(dxn1+2*dxn2)/dxn2

solve:
  FOR i=2 TO nm2
    a(i,2)=a(i,2)-a(i,1)/a(i-1,2)*a(i-1,3)
    a(i,4)=a(i,4)-a(i,1)/a(i-1,2)*a(i-1,4)
  NEXT i
  a(nm2,4)=a(nm2,4)/a(nm2,2)
  FOR i=nm2-1 TO 1 STEP -1
    a(i,4)=(a(i,4)-a(i,3)*a(i+1,4))/a(i,2)
  NEXT i
  FOR i=1 TO nm2
    s(i+1)=a(i,4)
  NEXT i

  ON endcond GOTO end11,end22,end33

end11:
  s(1)=0 : s(n)=0 : GOTO coeff
end22:
  s(1)=s(2) : s(n)=s(nm1) : GOTO coeff
end33:
  s(1)=((dx1+dx2)*s(2)-dx1*s(3))/dx2
  s(n)=((dxn2+dxn1)*s(nm1)-dxn1*s(nm2))/dxn2

coeff:
  FOR i=1 TO nm1
    dx1=x(i+1)-x(i)
    a3(i)=(s(i+1)-s(i))/(6*dx1)
    a2(i)=s(i)/2
    a1(i)=(y(i+1)-y(i))/dx1-(2*dx1*s(i)+dx1*s(i+1))/6
    a0(i)=y(i)
  NEXT i

calculate:
  INPUT "Enter interval between points "; dx
  PRINT "x-limits on file were : ",x(1),x(n)
  INPUT "Enter new x-limits "; x1,x2
  INPUT "Enter name of output file "; f$
  OPEN "out",#2,f$

```

```

FOR i=1 TO nm1
  xx=x1-x(i)
  WHILE x1<x(i+1)
    yy=a0(i)+a1(i)*xx+a2(i)*xx*xx+a3(i)*xx*xx*xx
    WRITE#2,x1,yy
    xx=xx+dx: x1=x1+dx
  WEND
NEXT i
xx=x1-x(nm1)
WHILE x1<=x2
  yy=a0(nm1)+a1(nm1)*xx+a2(i)*xx*xx+a3(i)*xx*xx*xx
  WRITE#2,x1,yy
  xx=xx+dx: x1=x1+dx
WEND
CLOSE#2
GOTO Enterdata

```


Program Graph - plots an internally defined function or a file from disk.

Joaquim Filipe Gaspar - Jan 1985 - **Naval Postgraduate School.**

```
DEFINT a-z : DEFSNG x,y,p : DIM xf(700),y(700),yf(700)
pi=3.141593 : YNF=3E+38
```

menudef:

```
  MENU 1,0,1,"Function"
    MENU 1,1,1,"Enter new function"
    MENU 1,2,2,"Use internal function"
    MENU 1,3,1,"Input new file from disk"
    MENU 1,4,0,"Use present file"
  MENU 2,0,1,"Resolution"
    MENU 2,1,1,"Very High"
    MENU 2,2,1,"High"
    MENU 2,3,2,"Medium"
    MENU 2,4,1,"Low"
  MENU 3,0,1,"Scaling"
    MENU 3,1,2,"Automatic"
    MENU 3,2,1,"Enter scaling factors"
  MENU 4,0,1,"X-Limits"
    MENU 4,1,1,"Enter x-limits"
  MENU 5,0,1,"Grid"
    MENU 5,1,2,"Yes"
    MENU 5,2,1,"No"
  MENU 6,0,1,"Title"
    MENU 6,1,1,"Enter title"
  MENU 7,0,1,"Run"
    MENU 7,1,0,"Start graph"
    MENU 7,2,0,"New graph"
    MENU 7,3,1,"Stop-List"
    MENU 7,4,1,"Quit"
  MENU ON
```

```
  res=4 : autoscale=1 : grid=1
```

Menuloop:

```
  IF xrange THEN MENU 7,1,1
  ON MENU GOSUB Menucheck
  GOTO Menuloop
```

Menucheck:

```
  ON MENU(0)GOSUB Function,Resolution,Scaling,Limits,Grid,Title,Start
  RETURN
```

Function:

ON MENU(1) GOTO Newfunction,Oldfunction,Newfile,Oldfile

Newfunction:

MENU RESET : STOP

Oldfunction:

foption=0

MENU 1,2,2 : IF fflag THEN MENU 1,4,1

RETURN

Newfile:

INPUT "Enter name of file "; f\$

OPEN "in",#1,f\$

i=0 : yfmin=YNF : yfmax=-YNF

WHILE NOT EOF(1)

i=i+1 : **INPUT#1,xf(i),yf(i)**

IF yf(i)>yfmax THEN yfmax=yf(i) : imax=i

IF yf(i)<yfmin THEN yfmin=yf(i) : imin=i

WEND

CLOSE#1

xfmin=xf(1) : xfmax=xf(i) : nx=i

fflag=1 : foption=1 : **MENU 1,2,1 : MENU 1,4,2**

RETURN

Oldfile:

foption=1 : **MENU 1,2,1 : MENU 1,4,2**

RETURN

Resolution:

res=2^{^(MENU(1)-1)}

FOR i=1 TO 4 : MENU 2,i,1 : NEXT i

MENU 2,MENU(1),2 : RETURN

Scaling:

IF MENU(1)=1 THEN autoscale=1 : MENU 3,1,2 : MENU 3,2,1 : RETURN

autoscale=0 : **MENU 3,1,1 : MENU 3,2,2**

INPUT "Enter x-axis step "; xstep

INPUT "Enter minimum y "; ymin

INPUT "Enter maximum y "; ymax

INPUT "Enter y-axis step "; ystep

IF foption THEN yrange=ymax-ymin

RETURN

Limits:

ON foption+1 GOTO limit1,limit2

limit1:

INPUT "Enter minimum x ";xmin : INPUT "Enter maximum x "; xmax

xrange=xmax-xmin

IF xrange=0 THEN limit1 ELSE RETURN

limit2:

```
PRINT "In present file, minim and max x's are : "; xfmin,xfmax
INPUT "Enter minimum x "; xmin : IF xmin<xfmin THEN limit2
INPUT "Enter maximum x "; xmax : IF xmax>xfmax THEN limit2
xrange=xmax-xmin
RETURN
```

Grid:

```
IF MENU(1)=1 THEN grid=1 : MENU 5,1,2 : MENU 5,2,1 : RETURN
grid=0 : MENU 5,2,2 : MENU 5,1,1 : RETURN
```

Title:

```
t$="" : INPUT "Enter title ";t$ : RETURN
```

Start:

```
IF MENU(1)=1 THEN Graph : RETURN
IF MENU(1)=3 THEN MENU RESET : STOP
IF MENU(1)=4 THEN SAVE "Graph" : SYSTEM
FOR i=1 TO 6 : MENU i,0,1 : NEXT i : MENU 7,2,0
CLS : CALL TEXTSIZE(12) : RETURN
```

Graph:

```
FOR i=1 TO 6 : MENU i,0,0 : NEXT i
CLS
ON foption+1 GOTO graph1,graph2
```

graph1:

```
  i=0
  IF autoscale=1 THEN ymax=-YNF : ymin=YNF
  FOR graphx=4 TO 488 STEP res
    i=i+1
    x=xmin+xrange*(graphx-4)/484
    GOSUB Fx
    IF autoscale=0 THEN 30
    IF y(i)>ymax AND ABS(y(i)<>YNF) THEN ymax=y(i)
    IF y(i)<ymin AND ABS(y(i)<>YNF) THEN ymin=y(i)
30  NEXT graphx
    yrange=ymax-ymin : ni=i-1
    GOTO setitle
```

graph2:

```
  i=1
  WHILE xf(i)<xmin
    i=i+1
  WEND
  ii=i : xmin=xf(i)
```

```

i=nx
WHILE xf(i)>xmax
  i=i-1
WEND
ifn=i : xmax=xf(i) : xrange=xmax-xmin
IF autoscale THEN ymax=yfmax : ymin=yfmin : yrange=ymax-ymin

settitle:
  CALL MOVETO(100,20) : PRINT t$;

xlabel:
  CALL TEXTSIZE(9)
  LINE(4,4)-(4,284) : LINE(4,284)-(488,284)
  IF autoscale THEN xstep=xrange/4
  FOR x=xmin+xstep TO xmax STEP xstep
    graphx=-484*(xmin-x)/xrange+4
    PSET(graphx,283)
    IF grid=0 THEN 40
    FOR graphy=280 TO 4 STEP -4
      PSET(graphx,graphy)
    NEXT graphy
40  CALL MOVETO(graphx-12,295)
    IF x<>xmax THEN PRINT x;
  NEXT x

ylabel:
  IF autoscale THEN ystep=yrange/4
  FOR y=ymin TO ymax STEP ystep
    graphy=280*(ymin-y)/yrange+284
    PSET(5,graphy)
    IF grid=0 THEN 50
    FOR graphx=9 TO 486 STEP 4
      PSET(graphx,graphy)
    NEXT graphx
50  CALL MOVETO(6,graphy-2)
    PRINT y;
  NEXT y

Plot:
  ON foption+1 GOTO plot1,plot2

plot1:
  FOR i=1 TO ni : IF (y(i)>ymax OR y(i)<ymin) THEN NEXT i
  gy=280*(ymin-y(i))/yrange+284
  gx=4+(i-1)*res : i=0
  FOR graphx=4 TO 488 STEP res
    i=i+1

```

```

        IF (y(i)>ymax OR y(i)<ymin) THEN flagy=0 : GOTO 5
        flagy=flagy+1 : graphy=280*(ymin-y(i))/yrange+284
        IF flagy>1 THEN LINE(gx,gy)-(graphx,graphy)
        gx=graphx : gy=graphy
5    NEXT graphx
    MENU 7,2,1
    RETURN

```

```

plot2:
    gx=-484*(xmin-xf(ii))/xrange+4
    gy=280*(ymin-yf(ii))/yrange+284
    FOR i=ii TO ifn
        graphx=-484*(xmin-xf(i))/xrange+4
        graphy=280*(ymin-yf(i))/yrange+284
        LINE(gx,gy)-(graphx,graphy)
        gx=graphx : gy=graphy
    NEXT i
    MENU 7,2,1
    RETURN

```

```

Fx:
    y(i)=EXP(-x*x)
    RETURN

```

INITIAL DISTRIBUTION LIST

	No. Copies
1. Defense Technical Information Center Cameron Station Alexandria, Virginia 22304-6145	2
2. Library, Code 0142 Naval Postgraduate School Monterey, California 93943-5100	2
3. Dr. Roland Garwood Naval Postgraduate School, Code 68Gd Monterey, California 93943	3
4. Dr. Peter Muller Department of Oceanography University of Hawaii 1000 Pope Road Honolulu, HI 96822	1
5. Dr. Stefan Hastenrath Department of Meteorology University of Wisconsin Madison, Wisconsin 53701	1
6. Mr. Patrick Gallacher Naval Postgraduate School, Code 68Ga Monterey, California 93943	1
7. Capitão tenente Joaquim Gaspar Divisão de Oceanografia Física Instituto Hidrográfico Rua das Trinas, 49 P - 1296 Lisboa CODEX Portugal	1
8. Biblioteca Instituto Hidrográfico Rua das Trinas, 49 P - 1296 Lisboa CODEX Portugal	1

- | | | |
|-----|---|---|
| 9. | Departamento de Oceanografia
Faculdade de Ciências de Lisboa
Rua da Escola Politécnica, 58
Lisboa
Portugal | 1 |
| 10. | Direcção do Serviço de Instrução e Treino
Praça do Comércio
1188 Lisboa CODEX
Portugal | 1 |
| 11. | Departamento de Oceanografia
Instituto Nacional de Meteorologia e Geofísica
Rua C , Airoporto de Lisboa
Lisboa
Portugal | 1 |

END

FILMED

11-85

DTIC